CANCER

ARAF suppresses ERBB3 expression and metastasis in a subset of lung cancers

Juliane Mooz[1], Kristina Riegel[1], Hari PS[2], Anguraj Sadanandam[2], Federico Marini[3,4], Matthias Klein[5], Ulrike Werner[6], Wilfried Roth[7], Annett Wilken-Schmitz[8], Irmgard Tegeder[8], Krishnaraj Rajalingam[1,9]*

RAF kinases are highly conserved serine/threonine kinases, and among the three RAF isoforms (ARAF, BRAF, and CRAF), the pathophysiological relevance of ARAF is not well defined. Here, we show that patients with lung cancer exhibit low expression of ARAF, which is associated with lymph node metastasis and poor patient survival. We uncover that depletion of ARAF promotes anchorage-independent growth and metastasis through activation of AKT signaling in a subset of lung cancer cells. We identified that loss of ARAF was associated with an increase in ERBB3 expression in a kinase-independent manner. ARAF suppressed the promoter activity of ERBB3, and reconstitution of ARAF in ARAF-depleted cells led to the reversal of enhanced ERBB3-AKT signaling. Furthermore, ARAF inhibited neuregulin 1 (hNRG1)–mediated AKT activation through controlling ERBB3 expression via the transcription factor KLF5. Our results disclose a critical dual role for ARAF kinase in the negative regulation of ERBB3-AKT signaling, thereby suppressing tumor metastasis.

INTRODUCTION

Lung cancer remains one of the leading causes of death among human cancers, and mutations in the *KRAS* oncogene are detected in nearly 30% of lung carcinomas (*1*). Attempts to target KRAS directly have gained momentum recently, and some of the drugs have entered clinical trials, especially the ones targeting the KRASG12C mutants (*2*). However, since RAS is very difficult to target by drugs, the major focus of current therapeutic approaches is still on the downstream kinases to counter RAS-mediated tumors. Among the several RAS effectors, RAF kinases have been intensively studied, and several small-molecule inhibitors have been developed that target these kinases to treat RAS-driven tumors (*3*). The RAF family of serine/threonine kinases consists of the three isoforms ARAF, BRAF, and CRAF, which undergo homo- and heterodimerization for their activation (*2*, *3*). RAF kinases [mitogen-activated protein kinase kinase kinase (MAP3K)], in turn, directly phosphorylate and activate MEK1/2 kinase (MAP2K), which culminates in the activation of extracellular signal–regulated kinase 1/2 (ERK1/2) (MAPK) by direct phosphorylation, thus completing the three-tier MAPK cascade (*4*, *5*). This classical MAPK cascade contributes to fundamental cellular processes such as proliferation, migration, differentiation, and cell survival (*6*). The mechanisms driving the activation of RAF kinases have been intensively studied and involve a multistep process including a series of phosphorylation and dephosphorylation events at the plasma membrane, as well as their dimerization as a key event (*2*, *7*).

RAF proteins themselves are found mutated in cancers. Mutations in *BRAF* are detected in approximately 7% of human cancers, while mutations in *ARAF* and *CRAF* are rare (*8*). Drugs targeting the activated mutants of BRAF were initially very promising in clinical trials, especially when combined with immunomodulatory drugs (*9*). However, paradoxical reactivation of MAPK has been observed in patients with *RAS* mutations after treatment with BRAF inhibitors, due to inhibitor-induced formation of heteromeric RAF complexes, which prevents a durable response and necessitates the development of new targeting strategies (*10*). While most of the studies in this regard are focused on BRAF and CRAF, the pathophysiological relevance of ARAF is still relatively little studied. ARAF has the lowest kinase activity among the RAF isoforms and binds only weakly to activated RAS (*5*). However, depending on the cell type, ARAF homodimers can function as the driving MAP3K to activate MEK1/2 kinases (*11*). Only this year, a novel type II RAF inhibitor that targets RAF for antitumor therapy in RAS-mutant tumor was shown to be able to inhibit dimerized BRAF and CRAF, as well as monomeric BRAF, but to largely spare ARAF. Both kinase function and dimerization were required for ARAF-mediated resistance to the compound that is currently undergoing clinical trials (*12*). In addition, mutations in ARAF were recently identified that conferred resistance to belvarafenib, again in a dimer- and kinase-dependent manner. Belvarafenib, a RAF dimer (type II) inhibitor, is used in patients with BRAFV600E and NRAS-mutated melanoma. The identified ARAF mutants exhibited reduced sensitivity to a whole panel of type II RAF inhibitors, and therefore, ARAF mutations may serve as a mechanism of cancer cells to escape RAF dimer inhibitors (*9*).

Research over the past decade has shown that the ERK signaling pathway is not exclusively linear but rather that its components are embedded in a network of other signaling pathways to regulate many proteins outside the classical pathway. ARAF, for example, was found to inhibit apoptosis during epithelial differentiation by directly binding to serine/threonine-protein kinase 3 (STK3/MST2), and

[1]Cell Biology Unit, University Medical Center of the Johannes Gutenberg University Mainz, 55131 Mainz, Germany. [2]Division of Molecular Pathology, The Institute of Cancer Research, London, UK. [3]Institute of Medical Biostatistics, Epidemiology and Informatics, University Medical Center of the Johannes Gutenberg University Mainz, 55131 Mainz, Germany. [4]Center for Thrombosis and Hemostasis (CTH), University Medical Center of the Johannes Gutenberg University Mainz, Mainz, Germany. [5]Institute of Immunology, University Medical Center of the Johannes Gutenberg University Mainz, 55131 Mainz, Germany. [6]Indivumed GmbH, Hamburg, Germany. [7]Institute of Pathology, University Medical Center of the Johannes Gutenberg University Mainz, 55131 Mainz, Germany. [8]Institute of Clinical Pharmacology, Goethe-University, Medical Faculty, Frankfurt (Main), Germany. [9]University Cancer Center Mainz, University Medical Center Mainz, Mainz, Germany.
*Corresponding author. Email: krishna@uni-mainz.de

splice variants of ARAF have been shown to negatively regulate ERK1/2 pathway rather than to activate it (*10*, *13*). The pathophysiological relevance of ARAF is also underlined by cancer sequencing studies in lung adenocarcinomas that have identified high copy number gains and oncogenic driver mutations in *ARAF* as an indicator of sorafenib response (*14*). In addition, a recurrent gain-of-function mutation in ARAF (ARAFS214P) has been recently identified in patients with anomalous lymphatic disease, which could be successfully treated with the MEK1/2 inhibitor trametinib (*15*). While the evidence obtained so far classifies *ARAF* as an oncogene, in the present work, we show that *ARAF* can also act as a tumor suppressor in lung cancers. Our results point to a dual role of ARAF in controlling the ERBB3-AKT signaling axis and tumor metastases. We found that ARAF suppresses activation of AKT kinase in a kinase-dependent manner, whereas it inhibits the transcription/expression of *ERBB3* in a kinase-independent manner, the latter contributing to cell survival through the modulation of the transcription factor KLF5. Last, in patients with lung cancer, low expression of *ARAF* correlated with lymph node metastasis and poor survival.

RESULTS

As the role of ARAF in the pathogenesis of human cancer is not well studied, we assessed the expression of *ARAF* mRNA in publicly available datasets of The Cancer Genome Atlas (TCGA) across various cancers. *ARAF* mRNA was down-regulated in a subset of human cancers including lung cancers (Fig. 1A). Non–small cell lung carcinoma (NSCLC) accounts for almost 85% of lung cancers and remains a leading cause of cancer-related deaths. NSCLCs are divided into three main subtypes: Adenocarcinoma (LUAD), squamous cell carcinoma (LUSC), and large cell carcinoma (LCC), with LUAD and LUSC being the two most frequently occurring subtypes, accounting for more than 70% of cases. Here, the analysis of normal and tumor tissue datasets from TCGA revealed that ARAF kinase is significantly down-regulated in LUADs ($P = 2.011 \times 10^{-5}$) and LUSCs ($P < 2.2 \times 10^{-16}$) (Fig. 1A). In LUADs, ARAF is down-regulated regardless of the mutation status of *epidermal growth factor receptor* (*EGFR*) (Fig. 1B) or *KRAS* (Fig. 1C). In addition, lower expression of *ARAF* mRNA correlated with low survival probability in patients with LUAD in TCGA (Fig. 1D). We further performed analysis on LUAD samples of GSE37745 that confirmed the correlation between ARAF and survival (fig. S1A). Our undertaking to investigate *ARAF* expression in relation to tumor stage using the GSE37745 and TCGA database revealed no correlation between *ARAF* expression and LUAD tumor progression (fig. S1, B and C). Since *ARAF* is an X-linked gene (Xp11.3), we additionally questioned whether there are relevant gender differences. However, analysis of TCGA data showed no gender-specific gene expression in LUADs (fig. S1D).

The reduced expression of *ARAF* in lung tumors and the concomitant correlation of low *ARAF* expression with low survival prompted us to further investigate whether ARAF might have a tumor-suppressive role in the pathogenesis of lung cancers such as LUADs and LUSCs. Therefore, we performed immunohistochemical (IHC) analysis of ARAF protein expression in tumor and adjacent normal tissue of LUADs and LUSCs (Fig. 2A). On the basis of the H-scores, IHC staining revealed that a small population in both subgroups of NSCLC had positive ARAF staining (Fig. 2B). Thus, of 84 tumor tissue samples where ARAF staining could be analyzed, 70 samples had H-scores between 0 and 50 and were consequently defined as ARAF negative. In addition, we studied the ARAF H-scores in relation to the clinically observed lymphatic metastases. More than half of the patients whose samples were negative for ARAF (H-score < 50) showed metastases to lymph nodes (Fig. 2C).

To further extend our study on the contribution of ARAF to lung cancer pathogenesis, we used lung cancer cells for the following experiments, including the well-studied LUAD cell line A549 (*11*), where we have previously shown that ARAF functions as an obligatory MAP3K. Although A549 cells carry a KRASG12S mutation, they have been shown to be sensitive to lapatinib, which targets HER2 amplified in this cell line (*16*). Consequently, A549 cells are not driven by KRAS, regardless of the G12S mutation. Since cancer patient survival is strongly correlated with metastasis and many of the analyzed patients exhibited lymph node metastases with a concomitant negative staining for ARAF, we set out to examine whether and how ARAF contributes to features important for tumor metastasis. Therefore, we established a stable knockdown of *ARAF* in A549 cells and confirmed that ARAF was critically required for MAPK activation in these cells, because ERK1/2 activation was reduced after ARAF depletion (Fig. 3A). To evaluate their ability to resist anoikis, to extravasate into the lung, and to form micrometastases, we injected them intravenously via the tail vein in NMRI nude mice (Fig. 3, B to D). The occurrence of lung colonization was strongly increased in mice injected with ARAF-depleted cells (Fig. 3, B to D), suggesting that ARAF suppressed tumor spreading to the lung. We were then interested whether the observed phenotype was dependent on the kinase activity of ARAF. Therefore, we performed reconstitution experiments where we stably reconstituted ARAF-depleted A549 cells with ARAF wild type (WT), kinase-active ARAF-DD (ARAFY301D/Y302D, analogous to CRAFY340D/Y341D), or with the dimer-deficient ARAF-R362H construct. As shown in previous publications, the ARAF-R362H mutation prevents both homo- and heteromerization of ARAF with CRAF and impairs the catalytic activity of ARAF (*11*, *17*), making it a kinase-deficient mutant. To reconfirm that this dimer-deficient mutant lacks catalytic activity, we again performed kinase assays using other kinase-deficient variants (ARAF-K336M and ARAF-S432A) for comparison. All three kinase-deficient mutants inhibited the induction of MEK1 phosphorylation despite similar efficiencies of ARAF immunoprecipitation (IP) (fig. S2A). Consistent with published observations (*12*), expression of WT and kinase-active ARAF-DD constructs, but not the dimer-deficient ARAF-R362H construct, led to the activation of MEK1/2 and ERK1/2 kinases in the stably reconstituted ARAF-depleted A549 cells (Fig. 4A).

Since anchorage-independent growth is a hallmark of metastatic cancer cells, we performed in vitro soft agar colony formation assays. Notably, in A549 cells, knockdown of only *ARAF*, but not *BRAF* and *CRAF*, resulted in increased numbers of colonies (fig. S2B). Reconstitution of ARAF-depleted cells with ARAF and ARAF-DD reduced their ability to grow anchorage independently, whereas expression of the kinase-deficient mutant had no effect on the ability to form colonies (Fig. 4B). The protein levels and the RNA levels of reconstituted ARAF-WT and ARAF-R362H were comparable to the endogenous ARAF levels detected in shControl cells (fig. S2, C and D). This precludes that differences in ARAF levels might have influenced the outcome of the experiments performed here. The in vitro reconstituted cells were then injected into the tail veins of NMRI nude mice. As expected, reexpression of ARAF in shARAF cells almost entirely eliminated their potential to induce lung tumor

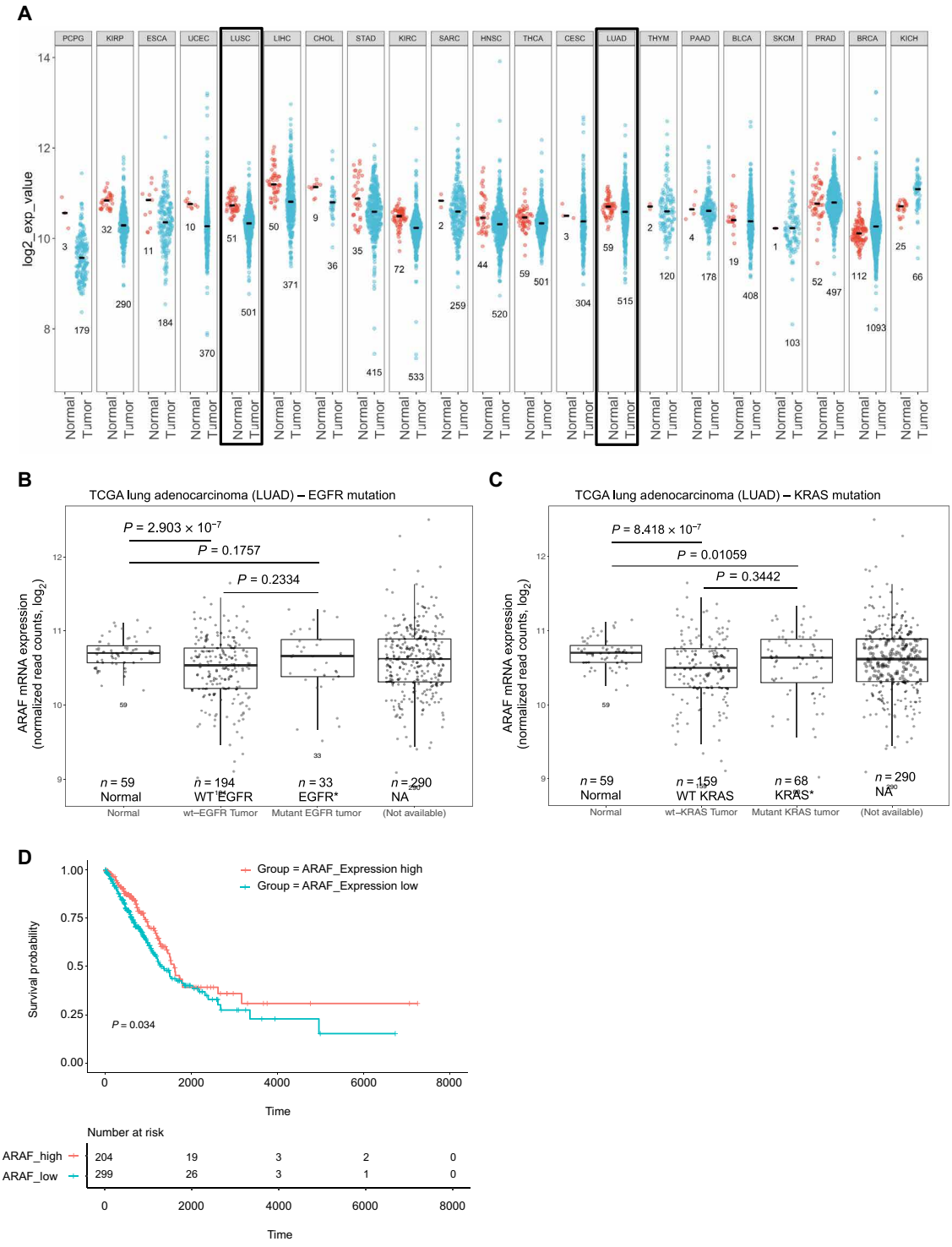

Fig. 1. *ARAF* expression is down-regulated in a variety of tumor tissues. (**A**) RNA-seq data for tumor and adjacent normal tissues were obtained from TCGA via curated TCGA Data, and *ARAF* expression values are plotted as $\log_2$-normalized reads (with addition of a pseudocount of 1). Boxplots show distribution of expression in all samples (range) and the number of samples at each expression level. (**B** and **C**) *ARAF* expression in TCGA LUAD patients that were stratified according to their *ARAF* mRNA levels and their mutation states (B) *EGFR* and (C) *KRAS*, respectively. (**D**) Low *ARAF* expression is correlated with poor prognosis of patients with lung cancer (LUAD). Kaplan-Meier survival curves were obtained from TCGA. *n*, total number of patients; 503 with a significant *P* value of 0.03.

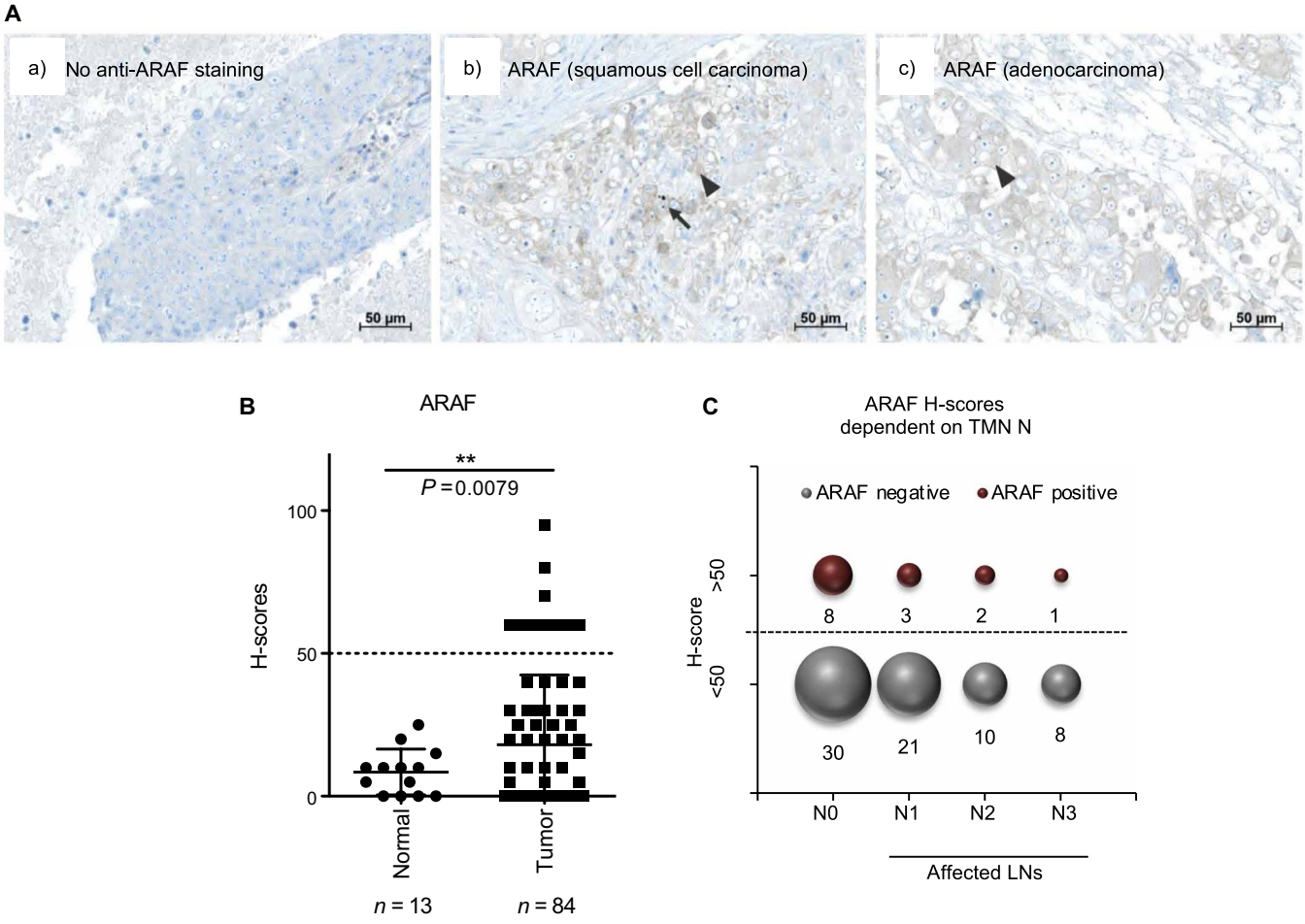

Fig. 2. *ARAF* expression in lung NSCLCs. (**A**) IHC staining of ARAF and analyses of NSCLC tumor and adjacent normal tissue were performed using tissue microarrays (TMAs) (as described in Materials and Methods). Shown are representative images of no anti-ARAF staining of tumor cells (a, H-score = 0), of an ARAF staining of a LUSC tissue sample (b, H-score = 20), and of a LUAD tissue sample (c, H-score = 80). The arrow highlights anthracosis, and the arrowheads show weak cytoplasmic anti-ARAF staining of tumor cells. (**B**) The ARAF H-score was calculated on the basis of the percentages of weakly, moderately, and strongly stained tumor cells in primary tumor samples ($n = 84$) and normal adjacent epithelial cells ($n = 13$) as described in Materials and Methods. Results are presented as means ± SD. An unequal variance Welch *t* test was performed (**P value of 0.0079). (**C**) ARAF H-scores of the tumor samples are illustrated dependent on the TMN-N classification of the corresponding patients. N0 indicates no signs of lymph node (LN) involvement, and patients with N1 to N3 have affected lymph nodes. ARAF stainings with H-scores < 50 are classified as ARAF negative, and ARAF stainings with H-scores > 50 are classified as ARAF-positive samples.

nodules (Fig. 4, C to E, and fig. S2, E to G). Cells expressing dimer-deficient ARAF-R362H largely phenocopied ARAF-depleted cells, suggesting a kinase- or dimerization-dependent effect of ARAF on the extravasation of these cells (Fig. 4, C to E, and fig. S2, E to G). On closer examination, the cells expressing ARAF-R362H exhibited a similar trend as shARAF cells on the induction of lung tumors, but they tended to be more susceptible to host-mediated defense and tumor shrinkage (fig. S2, E to G).

We then set out to investigate the mechanisms underlying the tumor-suppressive action of ARAF. To this end, we performed a kinase array with A549 lysates to detect the differentially activated kinases in control versus shARAF cells. We identified a strong activation of AKT kinase in shARAF cells (fig. S3, A and B), which we further confirmed by Western blot analysis (Fig. 5A, left). Intriguingly, IHC analysis revealed that the enhanced AKT activation upon ARAF depletion was also evident in the tumor cells that colonized the lung in our tail vein injection experiment (Fig. 5B), supporting the in vivo relevance of our finding. We further validated these observations in the lung cancer cell lines NCI-H1650 and NCI-H1437, both without *RAS* mutations, and consistently found that depletion of ARAF led to an increase in the activation of AKT kinase (Fig. 5A, right, and fig. S3C). Next, we aimed to evaluate AKT activation in cells lacking BRAF and CRAF. In contrast to ARAF-deficient A549 cells, small interfering RNA (siRNA)–induced double knockdown of *BRAF* and *CRAF* did not increase AKT phosphorylation (Fig. 5, C and D) but rather reduced it moderately. Although the induced AKT phosphorylation is weaker when *ARAF* knockdown was induced via siRNA instead of short hairpin RNA (shRNA), we were able to confirm the effect of *ARAF* knockdown on enhanced AKT activation with two different siRNAs (fig. S3D). Moreover, we verified in NCI-H1437 cells that AKT phosphorylation after shRNA-mediated knockdown of *BRAF* or *CRAF* is negligible (fig. S3C).

ARAF functions as an obligatory MAP3K in A549 cells, and in accordance with this, we observed a down-regulation of ERK1/2

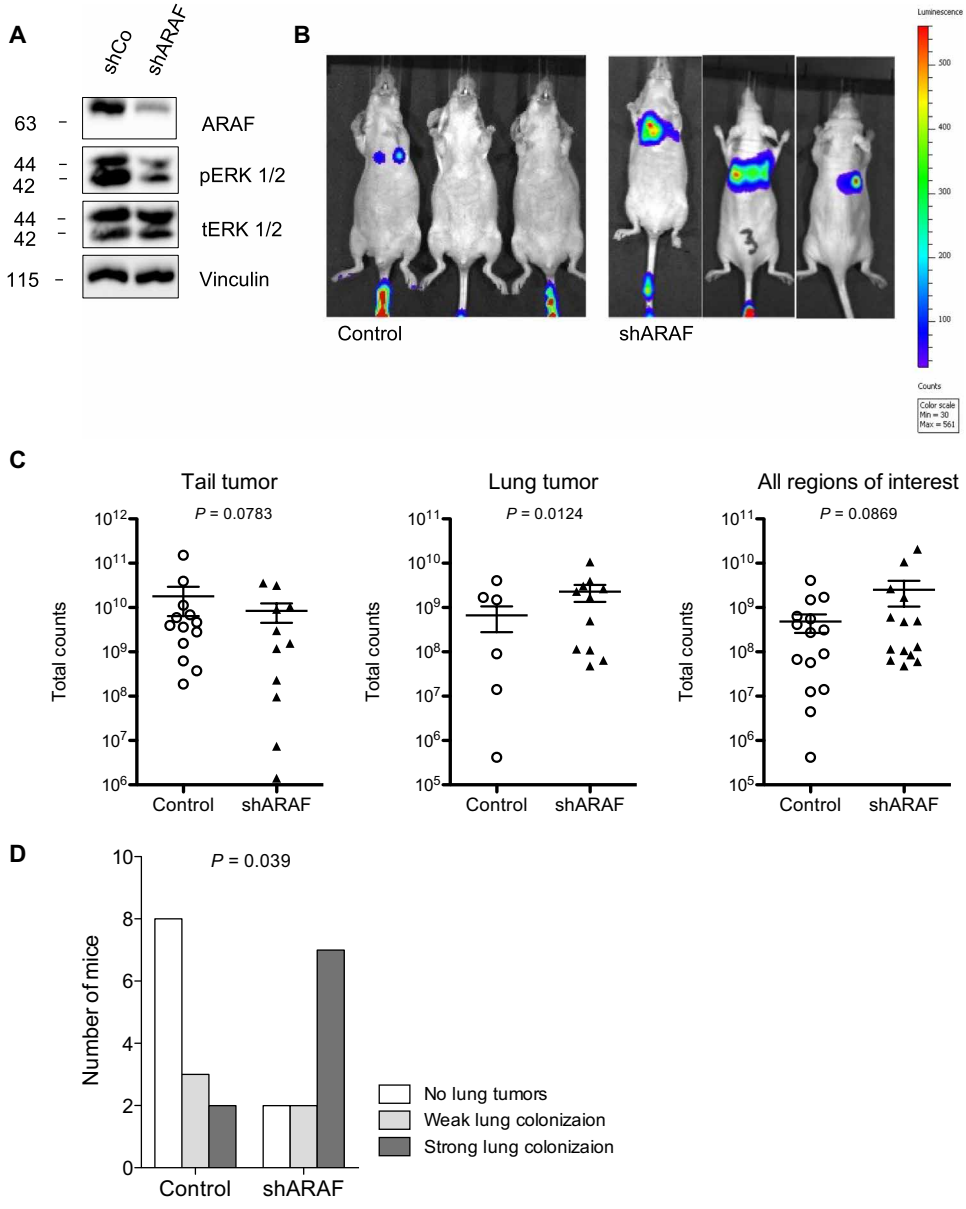

Fig. 3. ARAF down-regulation results in anchorage-independent growth and lung colonization in mice. (**A**) Western blotting of A549 control and ARAF-depleted cells. Cells (50,000) were plated into 12-well dishes and lysed 24 hours thereafter to verify the knockdown of ARAF and concomitant decrease in ERK 1/2 phosphorylation. (**B**) Loss of ARAF promotes lung metastasis in nude mice after tail vein injection of A549 cells, carrying CMV promoter–driven luciferase gene expression. Representative bioluminescence images show luciferase activity in tumor-bearing mice. Mice were injected with 1×10^6 control and ARAF-depleted (shARAF) A549 cells that were stably transfected with the firefly luciferase gene. Bioluminescence images were captured 10 min after injection of D-Luciferin intraperitoneally, 2 weeks after injection of tumor cells via the tail vein. The control group comprised 13 mice, while the shARAF group comprised 11 mice. (**C**) Scatterplots show the total counts of emitted photons in regions of interest (ROIs), which were automatically identified, software-aided. Each scatter shows one ROI. (**D**) To assess group differences, total counts were compared with Mann-Whitney *U* tests. In addition, the numbers of mice bearing lung metastases were compared with chi-squared statistics ($n_{control} = 13$; $n_{shARAF} = 11$; $P = 0.039$).

phosphorylation and/or activation in ARAF-depleted cells but not in BRAF/CRAF-depleted cells (Fig. 5E). Moreover, we used these cells to assess AKT activation under neuregulin (NRG1)–stimulating conditions, as NRG1 is known to transduce signaling via AKT. While NRG1 enhanced AKT phosphorylation in control cells, there was no additive effect on AKT phosphorylation in ARAF-depleted cells (Fig. 5E). In contrast, BRAF/CRAF-depleted A549 cells revealed only a marginal induction of AKT activation after NRG1 stimulation (Fig. 5E). We then performed complementation experiments and found, as expected, that the reconstitution of ARAF or ARAF-DD, but not ARAF-R362H, reduced the activation of AKT kinase in these cells (Fig. 5, F and G).

To test whether activation of AKT is a major driver of survival in A549 cells, we used MK-2206, an allosteric pan-AKT inhibitor, to shControl/shARAF-transfected A549 cells and performed soft agar colony formation assays. Treatment with MK-2206 impaired the anchorage-independent growth of both A549 control and ARAF-depleted cells (fig. S3E). In long-term clonogenic assays, we additionally

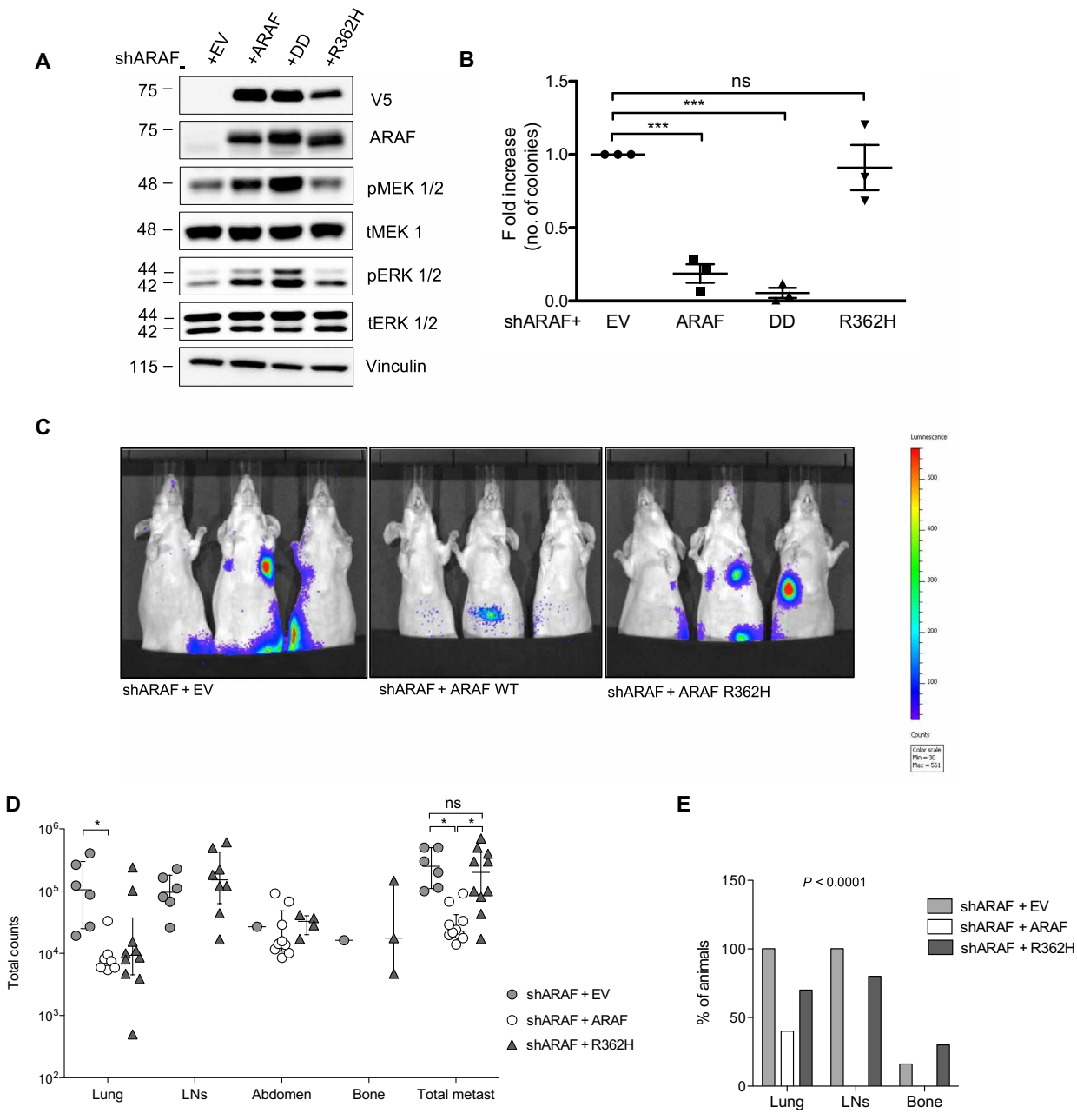

Fig. 4. Absence of ARAF kinase activity enables formation of metastasis in the lung and lymph nodes of nude mice. (**A**) Western blotting of A549 cells that were depleted for ARAF and reconstituted with either the empty vector (EV), WT ARAF (+ARAF), kinase-active (+DD), and kinase-deficient (R362H), respectively. Cells (30,000) were taken for Western blotting to evaluate ARAF (V5) overexpression and its effect on MAPK signaling or (**B**) mixed with 0.9% agarose and poured onto plates containing 1.5% agarose base for growing. Colonies were stained with crystal violet and photographed 14 days later. Quantification of colonies as fold change. Data are means ± SEM from three independent experiments. ***$P < 0.001$, one-way ANOVA with post hoc *t* tests using a correction of alpha according to Bonferroni. (**C**) Mice were injected with 1×10^6 stably expressing luciferase control and ARAF-depleted A549 cells reconstituted with WT ARAF (control), EV, and kinase-deficient mutant (R362H), respectively (from left to right). Representative images are shown. In vivo bioluminescence imaging was done 14, 17, and 21 days after injection of the tumor cells via the tail vein. Images were captured 10 min after injection of 100 μl of D-Luciferin (40 mg/ml) ($n = 6$). (**D**) Scatterplots show the total counts of emitted photons in ROIs at 17 days. ROIs were assigned to lung, lymph nodes, abdomen, and bones according to the anatomy and overlay with a standard mouse (implemented in LivingImage). Data are means ± SEM from six mice. *$P < 0.05$, one-way ANOVA with post hoc *t* tests using a correction of alpha according to Bonferroni. (**E**) Bar diagram shows the frequency of mice carrying metastases at the indicated sites 17 days after tumor cell injection. Chi-square $P < 0.0001$. ns, not significant.

observed reduced colonies when we treated A549 control and ARAF-depleted cells with GDC-941, an oral phosphatidylinositol 3-kinase (PI3K) inhibitor that acts upstream of AKT activation (*18*), or with the pan-PI3K inhibitor buparlisib (BKM-120) (fig. S3F). Together, these data indicate that AKT signaling has an important role in anchorage-independent survival.

We then generated transcriptome profiles of the *ARAF* knockdown and reconstituted cells described in Fig. 4 to identify factors

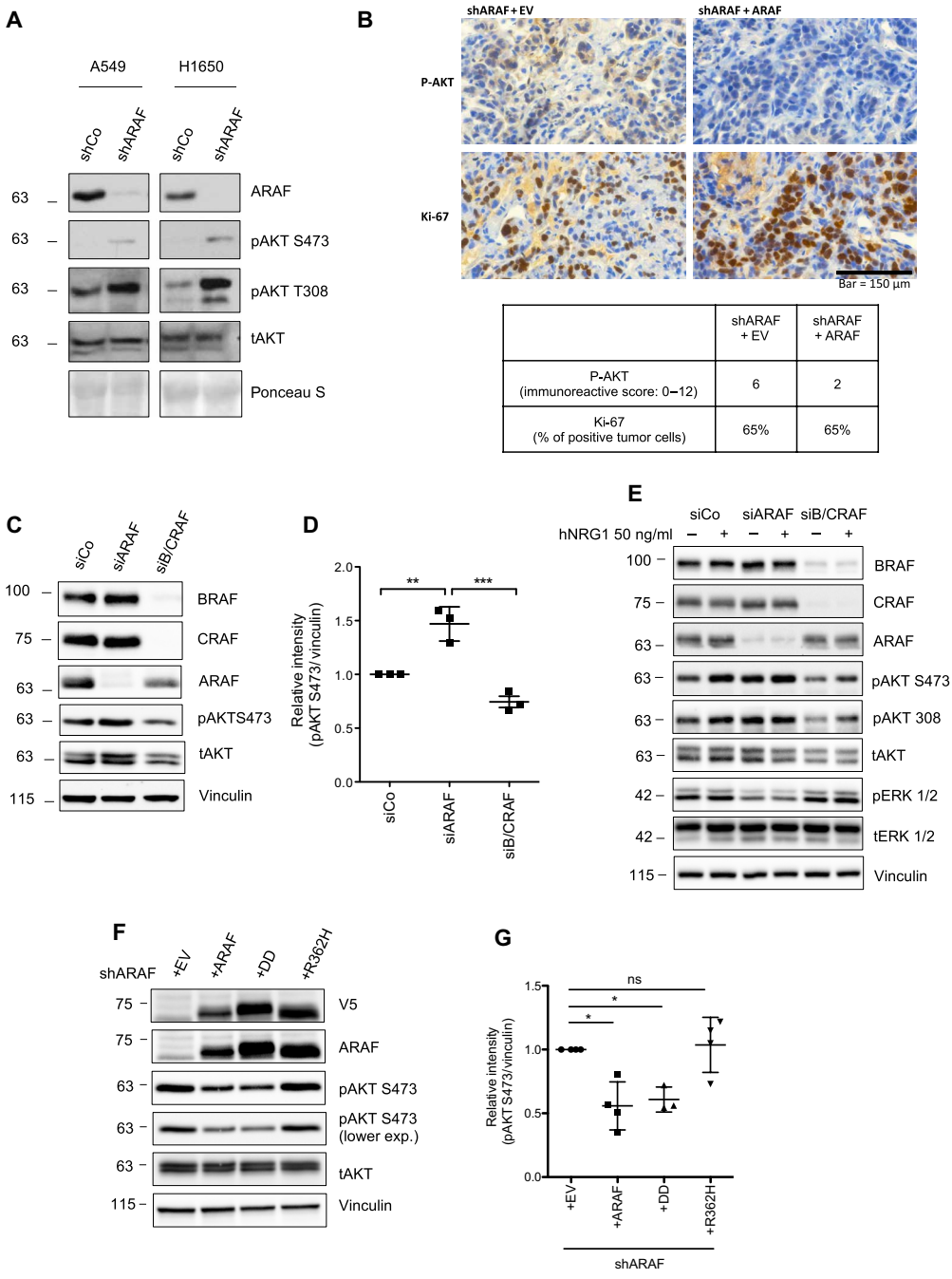

	shARAF + EV	shARAF + ARAF
P-AKT (immunoreactive score: 0–12)	6	2
Ki-67 (% of positive tumor cells)	65%	65%

Fig. 5. ARAF down-regulation results in persistent phosphorylation of Akt. (**A**) Western blotting for NSCLC cell lines that either harbor WT *EGFR* (A549) or in which the *EGFR* gene is mutated (H1650). Stable knockdown of *ARAF* leads to the phosphorylation of AKT (T308, S473). p-, phosphorylated protein. (**B**) Tumor tissue was immunohistochemically stained with antibodies specific for p-Akt (top row) and the proliferation marker Ki-67 (bottom row). Immune-positive cells appear in brown. Scale bar, 150 µm. Table shows IHC scores based on semiquantitative assessment of p-Akt expression as described in Materials and Methods. (**C**) A549 cells (150,000) were depleted for various RAF isoforms using the reverse siRNA transfection protocol and lysed 48 hours later for Western blot analysis. Shown is a representative Western blot image depicting phosphorylation levels of AKT (S473) with vinculin serving as a loading control. t-, total protein. (**D**) Relative expression level of pAKT (S473) in RAF-depleted cells compared to siControl was calculated after normalization with vinculin (loading control) and is presented as mean fold change ± SD from three biological replicates ($n = 3$). *$P < 0.05$, **$P < 0.01$, and ***$P < 0.001$, one-way ANOVA, Bonferroni posttest. (**E**) A549 cells (150,000) were depleted for various RAF isoforms using the reverse siRNA transfection protocol and 48 hours later stimulated with the ERBB3 ligand hNRG1 for 10 min. Cells were subjected to SDS-PAGE analysis. The knockdown of individual RAF isoforms was confirmed, and phosphorylation levels of AKT (S473 and T308) and ERK 1/2 (Thr^{202}/Tyr^{204}) were monitored with vinculin serving as a loading control. (**F**) Representing Western blot analysis of AKT phosphorylation in A549 cells where ARAF was stably depleted (shARAF) or reconstituted with control hairpin (+EV), ARAF-WT (+ARAF), or ARAF kinase–deficient (+R362H). (**G**) Relative intensity values of phosphorylated AKT were calculated after normalization with loading control and are presented as mean fold change ± SD from four biological experiments ($n = 4$) except for shARAF + DD where three biological replicates are depicted ($n = 3$).

that are differentially regulated by ARAF and its kinase activity (tables S1 to S3). To confirm reproducibility of the results, we checked the relationships between the three groups by principal components analysis (PCA). We observed that the samples within each biological group clustered well together (fig. S4A), so with that, we proceeded with differential gene expression analysis (fig. S4B). To get an idea of which cellular pathways were affected by the presence or absence of ARAF, the differentially expressed genes were further assigned into Gene Ontology (GO) categories of biological processes, cellular components, and molecular functions. The genes enriched in the cluster of biological processes were related to functions such as, but not limited to, positive regulation of cell motility, cell matrix adhesion, positive regulation of epithelial cell migration, cell junction adhesion, and epithelial-to-mesenchymal transition (Fig. 6A). GO analysis further revealed that some factors contributing to the regulation of AKT signaling, cell migration, and cell adhesion are deregulated in these cells in an ARAF kinase–dependent manner and some in a kinase-independent manner (Fig. 6B and fig. S4, C to E).

Subsequently, we analyzed factors that directly or indirectly contributed to AKT signaling in cells that lacked *ARAF* kinase expression. Intriguingly, expression of *ERBB3*, a kinase-impaired receptor tyrosine kinase, was substantially down-regulated when ARAF or ARAF-R362H was reexpressed in ARAF-depleted cells (Fig. 6B and fig. S5A). The enhanced expression of *ERBB3* in an ARAF-depleted background was verified by real-time polymerase chain reaction (PCR) and Western blot analysis (Fig. 6, C and D). Consistent with the RNA sequencing (RNA-seq) analysis, reconstitution of ARAF-depleted cells with ARAF or with different kinase-deficient mutants (ARAF-R362H, ARAF-S432A, and ARAF-K336M) reversed the expression of *ERBB3*, suggesting a regulatory mechanism independent of ARAF kinase activity (Fig. 6E). Since reconstitution of ARAF-depleted cells with the kinase-active ARAF-DD mutant also suppressed *ERBB3* expression, we can further conclude that ARAF activation does not interfere with the underlying regulatory mechanism (Fig. 6D). In addition, we tested how BRAF/CRAF depletion affects *ERBB3* expression in A549 cells. While siRNA-mediated *ARAF* knockdown strongly enhanced *ERBB3* expression, double knockdown of *BRAF* and *CRAF* had only a mild effect on its expression (Fig. 6F), again suggesting a strong ARAF-dependent effect.

ERBB3 has been shown to promote tumor initiation and progression and to contribute to cell survival and drug resistance through strong activation of PI3K/AKT signaling (*19*). TCGA data analysis showed a significant increase in *ERBB3* expression in lung adenocarcinomas irrespective of *KRAS* or *EGFR* mutation status (fig. S5, B and C). In a subset of lung cancer cell lines that harbor activating *KRAS* mutations, no effect of ARAF depletion on *ERBB3* expression could be observed (fig. S5, D and E). In contrast, three of four LUAD cell lines that are WT for KRAS showed increased *ERBB3* expression upon siRNA-mediated silencing of *ARAF* (fig. S5, F and G), suggesting that the regulation is context- and cell type–dependent. To gain further insight into how *ARAF* expression affects AKT activation and *ERBB3* expression in vivo, we extended our IHC analysis described in Fig. 2 and stained the corresponding tissue samples for ERBB3 and pAkt (Fig. 7, A and B). Evaluation of H-scores revealed that only 12 of 45 tumor tissue samples showed a positive staining for pAKT (Fig. 7C), while 20 of 47 tumor tissue samples were ERBB3 positive (H-score > 50) (Fig. 7E). In addition, we further examined pAKT and ERBB3 H-scores in tumor patient samples that were negative for ARAF (H-score < 50). Here, we observed that there are subgroups of patients who indeed show an association of low ARAF levels with high pAKT (Fig. 7D) and high ERBB3 levels (Fig. 7F).

Last, we tested in a luciferase assay whether *ARAF* expression contributes to the promoter activity of *ERBB3*. After confirming the successful knockdown of *ARAF* and the reconstitution of ARAF constructs in the presence of the GLuc-ON promoter reporter, we demonstrated that *ERBB3* promoter activity is enhanced upon ARAF depletion (Fig. 8, A and B). To test whether blockade of ERBB2/3 signaling affects cell proliferation and survival, we assessed the effects of the highly selective ERBB2/3 inhibitor sapitinib. As shown in fig. S6A, treatment with sapitinib inhibits ERBB3 phosphorylation in A549 control cells and in ARAF-depleted cells. The inhibition of ERBB3 activation further results in decreased phosphorylation of AKT at S473, although it was more pronounced in ARAF-depleted cells. We next tested in three-dimensional soft agar colony formation assays to check whether sapitinib affects the average colony size of A549 control cells and ARAF-depleted cells (fig. S6B). Independent of the presence or absence of ARAF, sapitinib strongly decreased the size of the colonies, pointing to a strong dependency of A549 cells on ERBB2/3 signaling.

We were then interested in the underlying mechanism of how ARAF might regulate *ERBB3* promoter activity. For this purpose, we used our RNA-seq data (Fig. 6 and fig. S4) to identify regulated transcription factors (fig. S6C). In addition, we screened for transcription factor binding sites within the *ERBB3* promoter region (fig. S7, A and B). On the basis of this, we identified KLF5 as a potential transcription factor that might regulate *ERBB3* expression in an ARAF-dependent manner. *KLF5* mRNA levels were elevated in ARAF-depleted A549 cells (Fig. 8C). Furthermore, the shRNA-mediated knockdown of *KLF5* resulted in decreased *ERBB3* protein and mRNA levels (Fig. 8, D and E), showing that *KLF5* is indeed involved in the regulation of *ERBB3* expression. Intriguingly, the siRNA-mediated knockdown of *KLF5* prevented the induction of *ERBB3* expression after ARAF depletion. This KLF5/ARAF-dependent effect on *ERBB3* expression was evident at both the protein and mRNA levels (Fig. 8, F and G). Last, we verified by chromatin immunoprecipitation (ChIP)–qPCR analysis that KLF5 indeed binds to the *ERBB3* promoter and that KLF5 promoter binding is significantly enhanced in ARAF-depleted cells (Fig. 8H). Consequently, we identified KLF5 as a previously unknown transcription factor regulating *ERBB3* expression in an ARAF-dependent manner. FOXC1 is another transcription factor that was found to be elevated in NSCLC tissues and whose expression negatively correlated with patient survival (*20*). Concomitantly, we find that FOXC1 is up-regulated in ARAF-depleted cells (fig. S7C). However, in contrast to *KLF5*, *FOXC1* knockdown enhances *ERBB3* expression in A549 control cells. This negative correlation is interesting as *FOXC1* has a potential consensus sequence within the *ERBB3* promotor (fig. S7, A and B). Intriguingly, in ARAF-depleted cells, *FOXC1* knockdown did not further enhance *ERBB3* expression (fig. S7D).

We then assessed the role of ARAF in regulating AKT signaling in ligand-dependent activation of ERBB3 complexes. NRG1 binds to ERBB3/HER3, thereby inducing dimerization with ERBB2/HER2 and subsequent transphosphorylation of ERBB3, which transduces signaling via AKT and ERK effectors (*21*). As expected, NRG1 treatment induced ERBB3 and AKT phosphorylation independent of the presence or absence of ARAF, although the stimulatory effects were

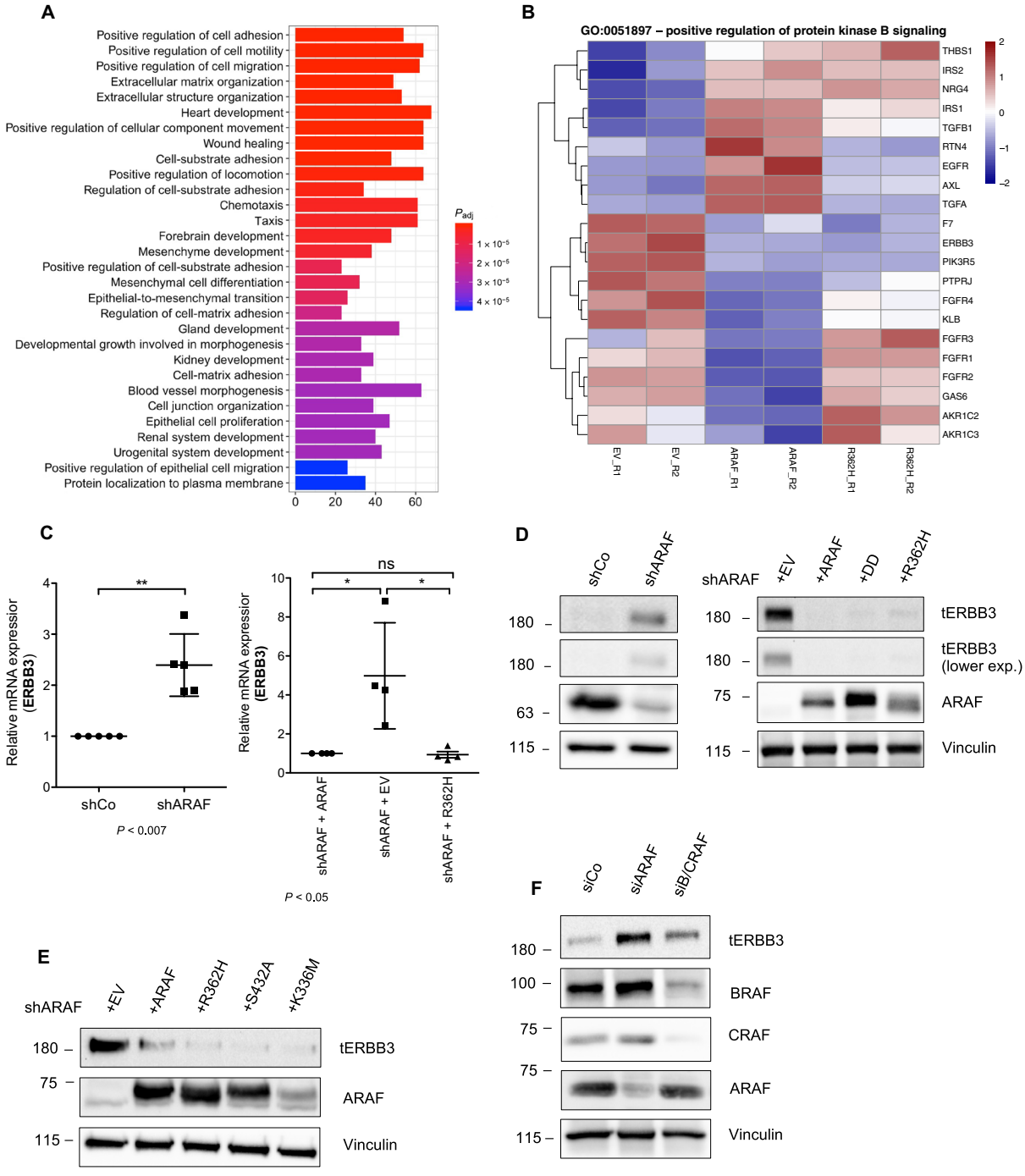

Fig. 6. ARAF down-regulation influences target gene expression in ERRB3 signaling. (**A**) Gene Ontology (GO) enrichment analysis of genes that are differentially expressed upon ARAF shRNA transduction (shARAF + EV) and reexpression of WT ARAF (shARAF + ARAF) in A549 cells. The selected pathways are mainly focused on extracellular matrix–related and biological adhesion molecules. (**B**) Signature heatmap for the genes associated with positive regulation of protein kinase B signaling (also known as Akt) in shARAF A549 cells reconstituted with EV, ARAF, or R362H, respectively. Plotted expression values are the *z* scores of regularized logarithm (rlog)–transformed counts, after library size normalization. (**C**) RT-PCR validation of ERBB3 mRNA expression levels in control (shCo) and ARAF-depleted (shARAF) A549 cells shown as means ± SD fold changes (left, $n = 5$) $^{**}P < 0.01$, paired *t* test, two-tailed. Right shows relative expression of *ERBB3* in shARAF + ARAF (control), shARAF + EV (knockdown), and shARAF + R362H A549 cells, respectively ($n = 4$). $^{*}P < 0.05$, one-way ANOVA with Bonferroni post hoc test. (**D**) Western blot analysis of A549 cells to determine ERBB3 protein expression as well as *ARAF* knockdown (left) and reconstitution with indicated ARAF mutants (right). Vinculin served as a loading control. Shown is one representative Western blot for at least three independent experiments. (**E**) Western blotting of ARAF-depleted A549 cells reconstituted with ARAF and different ARAF kinase–deficient mutants, respectively. ARAF and ERBB3 levels were monitored with vinculin as a loading control. (**F**) siRNA-induced knockdown of *RAF* isoforms was induced in A549 cells and verified by Western blot analysis. ERBB3 and vinculin expression was determined as well. Shown is a representative Western blot.

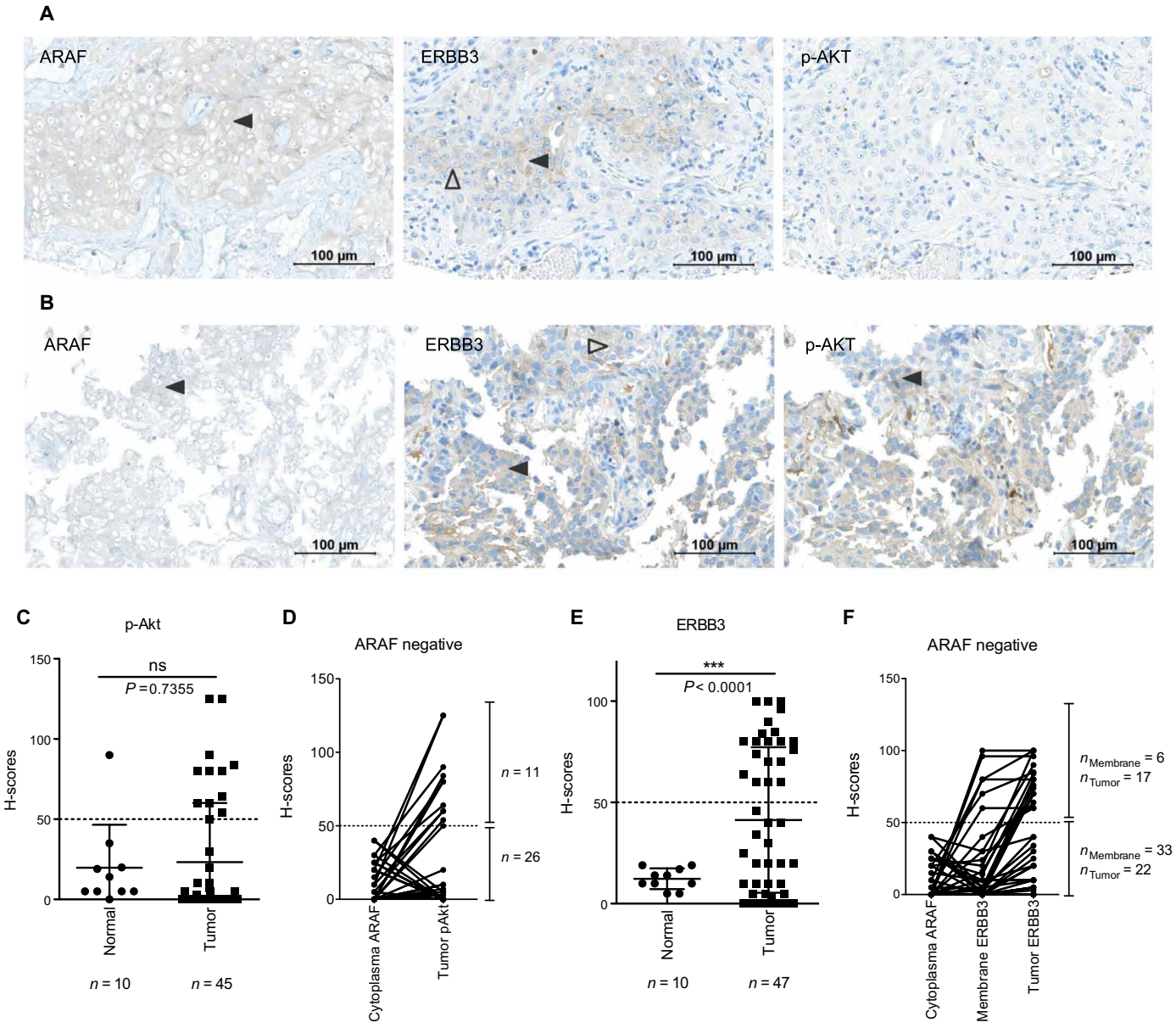

Fig. 7. p-AKT and *ERBB3* expression in lung NSCLCs. (**A**) IHC staining of p-AKT and ERBB3 in a human LUAD tumor sample that showed a negative staining for ARAF (H-score < 50). Staining was performed using TMAs as described in Materials and Methods. Arrowheads show weak cytoplasmic stainings, and the open arrowhead highlights weak membranous staining. Shown TMA is representative for patient samples that showed a negative staining of ARAF (H-score = 40), ERBB3 (H-score = 10), and p-AKT (H-score = 0). (**B**) Same as in (A), but with a human LUSC TMA, which is representative for patients with negative ARAF staining (H-score = 5), but positive ERBB3 (H-score = 74) and p-AKT (H-score = 60) staining. (**C**) The pAKT H-score was calculated as described in Materials and Methods based on the percentages of weakly, moderately, and strongly stained tumor cells in primary tumor samples ($n = 45$) and normal adjacent epithelial cells, pneumocytes ($n = 10$). Results are presented as means ± SD. An unequal variance Welch *t* test was performed ($P = 0.7355$). (**D**) The pAKT H-scores are presented in correlation to the ARAF H-scores that were below 50, thus representing tumor samples with an ARAF-negative staining. (**E** and **F**) Same as in (C) and (D), but H-scores of ERBB3 were analyzed. An unequal variance Welch *t* test was performed, indicating a significant difference in the ERBB3 H-scores between normal and tumor samples (***$P < 0.0001$).

more pronounced in an ARAF-depleted background (fig. S8A). In contrast to NRG1, stimulation with basic fibroblast growth factor (bFGF) and EGF induced ERK1/2 but not ERBB3 activation (fig. S8A). In at least three different lung carcinoma cell lines, ARAF depletion enhanced the phosphorylation of ERBB3/AKT under NRG1-stimulating but not EGF-stimulating conditions (fig. S8, B to D). In line with Fig. 6E, reexpression of ARAF WT or a kinase-active mutant in an ARAF-depleted background strongly reduced *ERBB3* expression, so that NRG1 stimulation resulted in only a weak activation of ERBB3 and AKT (Fig. 9A). These data suggest that the increase in *ERBB3* expression in ARAF-depleted cells also leads to a stronger induction of the downstream signaling pathway under stimulatory conditions. This, in turn, indicates that ARAF negatively regulates the ERBB3-AKT axis. To test whether the knockdown of *ERBB3*

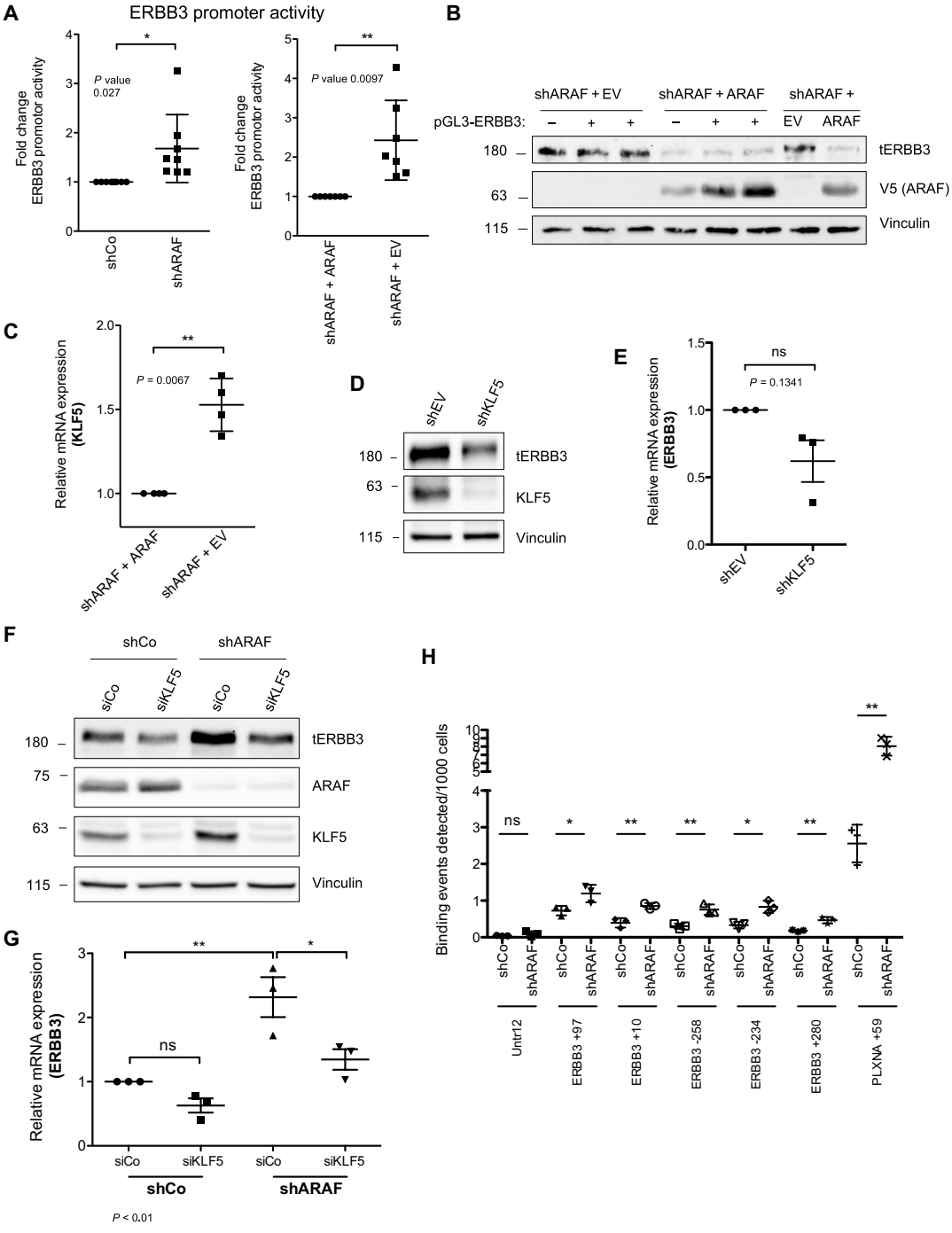

Fig. 8. ARAF regulates ERRB3 oncogenic signaling. (**A**) *ERBB3* promotor activity was determined in control (shCo) and ARAF-depleted (shARAF) A549 cells as well as in reconstituted ARAF-depleted A549 cells (shARAF + ARAF and shARAF + EV) in a luciferase promotor activity assay. Shown is the fold change in *ERBB3* promotor activity. The data are the means ± SD fold change in RLU of ARAF-depleted samples normalized to the control. Paired *t* test, two-tailed $*P < 0.05$ and $**P < 0.01$ with $n = 8$. (**B**) A representative Western blot of pGL3-ERBB3 (human ERBB3 gene promoter luciferase reporter plasmid)–transfected A549 cells used in (A) is shown, and ARAF knockdown efficiency and total ERBB3 protein level were monitored. (**C**) Relative *KLF5* mRNA levels were determined by RT-PCR in ARAF-depleted A549 cells reconstituted with ARAF and EV, respectively. Paired *t* test, two-tailed $**P < 0.01$ with $n = 4$. (**D**) Knockdown of *KLF5* was induced in A549 by shRNA, and knockdown efficiency as well as total ERBB3 levels were determined by Western blot analysis. A representative Western blot is shown. (**E**) Relative mRNA levels of ERBB3 were analyzed in KLF5-depleted A549 cells by RT-PCR. Paired *t* test, two-tailed with $n = 3$. (**F**) Control (shCo) and ARAF-depleted (shARAF) A549 cells were transfected with siRNAs to specifically knock down *KLF5*. Knockdown of *ARAF* and of *KLF5* was confirmed by Western blot analysis, and total ERBB3 protein level was analyzed. (**G**) Relative ERBB3 mRNA levels were determined by RT-PCR in control (shCo) and ARAF-depleted (shARAF) A549 cells that were additionally transfected with siControl and siKLF5, respectively. Shown as means ± SD fold changes ($n = 3$, $*P < 0.05$ and $**P < 0.01$, one-way ANOVA, Bonferroni posttest. (**H**) ChIP-qPCR analysis was performed as described in Materials and Methods. Shown are data from three biological replicates with a different set of primers while PLXNA+59 served as a positive control.

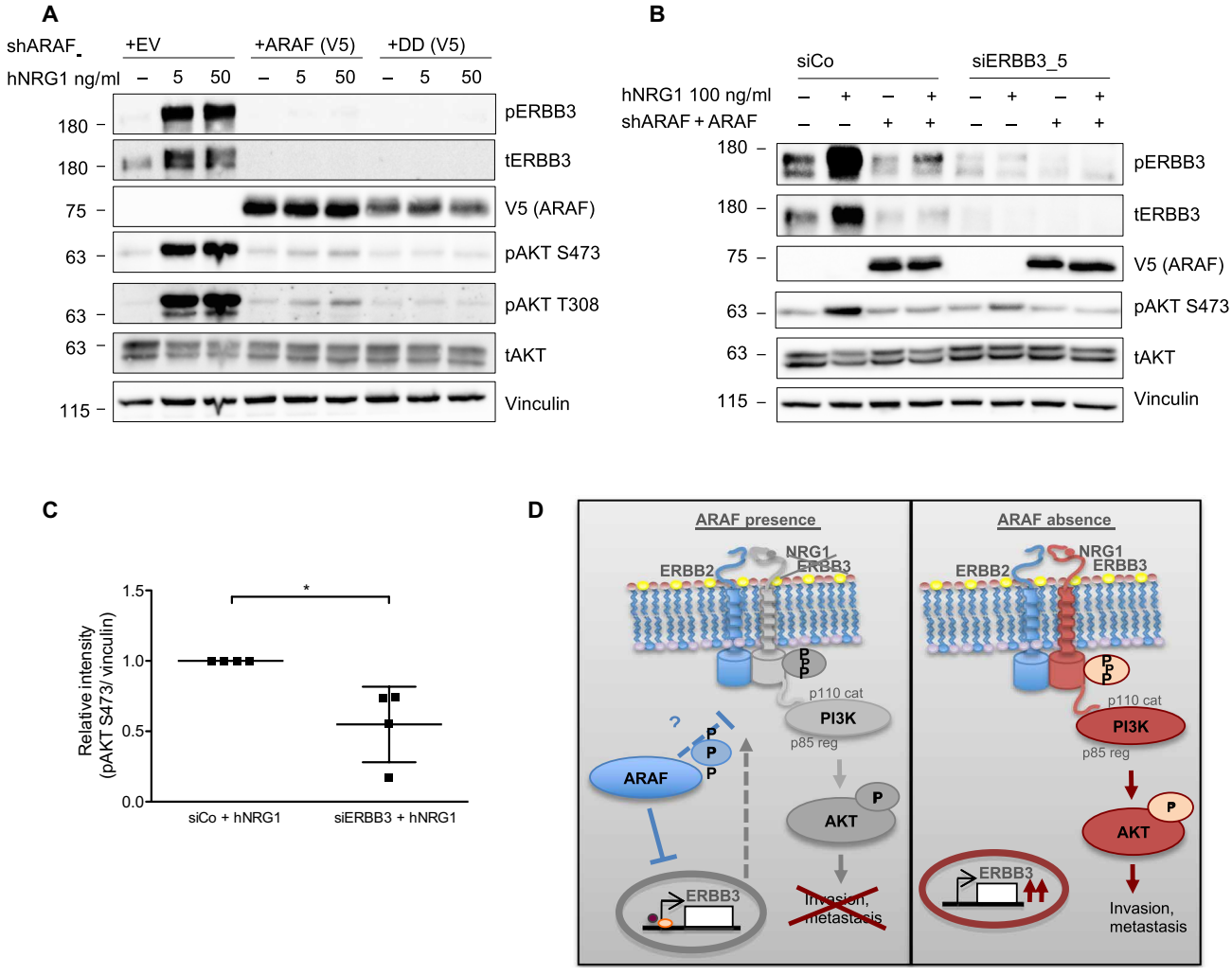

Fig. 9. ARAF regulates ligand-induced phosphorylation of AKT in an ERBB3-dependent manner. (**A**) A549 cells that were depleted for ARAF (+EV) and reconstituted with WT (+ARAF) and kinase-active (+ARAF-DD), respectively, were seeded in a 12-well dish at a density of 1×10^5 and stimulated 24 hours later with indicated concentrations of hNRG1 for 20 min. Phosphorylation levels of ERBB3 (Tyr^{1289}), AKT (S473), and T308 were monitored with vinculin serving as a loading control. The phospho blots of ERBB3 were stripped and probed for checking total ERBB3 levels. (**B**) A549 cells that were depleted for ARAF(+EV) or reconstituted with WT ARAF were transiently transfected with siRNA targeting ERBB3 (siERBB3) or control siRNA (siCo) and stimulated with hNRG1 (100 ng/ml) for 20 min before lysates were subjected to Western blotting and probed for indicated proteins with vinculin serving as a loading control. (**C**) Quantification of pAKT levels (S473) presented in (B) from ARAF-depleted cells silenced for ERBB3 compared to siControl treated with hNRG1 (100 ng/ml), respectively. Fold change values were calculated after normalization with internal loading control (vinculin), and four independent experiments ($n = 4$) are represented as means ± SEM. *$P < 0.05$, *t* test. (**D**) Illustration of the dual role of ARAF in the regulation of the ERBB3-AKT signaling axis and metastasis. ARAF kinase controls the promoter activity of ERBB3 and thus its expression in a kinase-independent manner. ARAF partially suppresses NRG1-ERBB3-AKT activation in a kinase-dependent manner. Loss of ARAF promotes ERBB3-AKT signaling and metastasis in a cell type–dependent manner.

would abolish ligand-induced PI3K/AKT signaling, we silenced *ERBB3* expression using siRNA in control versus ARAF-depleted cells. Compared to the corresponding control, AKT phosphorylation at S473 was reduced upon loss of ERBB3 in the NRG1-stimulated and ARAF-depleted cells, showing that the PI3K pathway is dependent on ERBB3 (Fig. 9, B and C).

It has been shown that RAF inhibition by MAPK pathway inhibitors results in increased *ERBB3* gene transcription in thyroid cancer cells (*22*). Furthermore, in melanoma cells, enhanced ERBB3 signaling promoted resistance to RAF pathway inhibitors (*23*). As ARAF down-regulation reduced MAPK signaling (Fig. 3A), we tested whether treatment with the MEK inhibitor trametinib leads to elevated ERBB3 levels in A549 cells. Trametinib treatment increased tERBB3 levels in the control cells only after 24 hours, whereas tERBB3 levels returned to basal levels after 48 hours of treatment. However, under *ARAF* knockdown conditions, tERBB3 levels were consistently increased at 24 and 48 hours, and trametinib treatment resulted only in a minor additive increase after 24 hours of treatment (fig. S9, A and B). These observations suggest that ARAF has a role in regulating *ERBB3* expression in an MAPK-independent manner. Together, our study revealed an important role of ARAF in suppressing ERBB3-AKT signaling in a dual kinase-dependent and kinase-independent manner through KLF5 (Fig. 9D). Considering that the kinase-deficient mutant mimicked the ARAF-depleted phenotype in our tail vein

injection in vivo experiment in terms of tumor onset and early growth, it may be concluded that the kinase-independent ERBB3-inducing aspect is possibly the predominant mechanism in vivo.

DISCUSSION

Targeting the components of the MAPK cascade remains a major strategy to combat RAS-driven tumors, and recent studies from the Barbacid laboratory confirmed that CRAF kinase is primarily required for driving KRAS-mediated tumorigenesis (*24*). In contrast to advances in the treatments targeting BRAF and CRAF, the role of ARAF kinase in driving tumorigenesis remains understudied since the intrinsic kinase activity of ARAF is relatively low compared to the other members of the RAF kinase family. We have previously identified a critical role for ARAF as key regulator of MAP3K in a subset of cancer cells. In these cells, ARAF homodimers were primarily responsible for the activation of MEK1/2 (*11*). Here, we present evidence that ARAF kinase is down-regulated in a subset of lung cancers and that depletion of ARAF promotes anchorage-independent growth and metastasis in a panel of cell lines in vitro and in vivo. These effects were not observed in cell lines driven by *KRAS* mutations; rather, the metastasis-suppressive effects of ARAF were evident in cells with WT or single-mutant *KRAS*. We found that ARAF negatively regulated the expression of *ERBB3* and that the depletion of ARAF promoted survival of the cells by reactivating the ERBB3-PI3K-AKT signaling axis. A previous study has shown that inactivation of *ERBB3* by siRNAs attenuated growth and invasiveness in A549 and other LUAD cell lines in which ERBB2/3 drives the signaling irrespective of *KRAS* mutations (*25*). While the activation of AKT signaling in ARAF-depleted cells was clearly dependent on its kinase activity, the suppression of metastasis or *ERBB3* expression was not entirely dependent on its kinase activity. While cells expressing a dimer-deficient mutant of ARAF phenocopied the loss of ARAF during the onset of metastasis, this effect faded beyond 14 days in an experimental metastasis mouse model, pointing to a slower metastatic growth rate. Consistently, LUAD patients with low *ARAF* expression have reduced overall survival probability, suggesting a possible tumor-suppressive role of ARAF kinase in a context- and cell type–dependent manner. This is in sharp contrast to BRAF kinase, which primarily exhibits pro-oncogenic properties. In lung cancers, further studies with bigger cohorts of patients carrying various subtypes are clearly warranted. CRAF kinase has been shown to have tumor-suppressive functions in hepatocellular carcinoma (*21*).

Unexpectedly, ARAF-mediated suppression of *ERBB3* expression was not dependent entirely on MEK1, a well-established downstream target of RAF kinases. Treatment with the potent MEK1/2 inhibitor trametenib failed to reverse high ERBB3 levels in ARAF-depleted cells. It is therefore highly pertinent to uncover ARAF-interacting proteins and previously unknown substrates that might be involved in establishing this phenotype. In this study, we identified KLF5 as a transcription factor that contributes to repression of *ERBB3* promoter activity downstream of ARAF. Whether ARAF relocates to the nucleus and directly binds to KLF5 or whether another player is involved needs to be determined. Noteworthy, we cannot exclude that other repressors of the *ERBB3* promotor such as CtBP1 and CtBP2 or FOXD3 play a role in this process (*22*, *23*).

ARAF suppressed the ERBB3-AKT signaling axis in response to NRG1, a known agonist of ERBB3, most likely by regulating *ERBB3* expression as observed in three different cell lines. Especially elevated ARAF levels seem to decrease ERBB3 responsiveness to NRG1, suggesting that the fine balance of *ARAF* expression might be a key determinant. Further studies are needed to assess whether ARAF suppresses the NRG1 autocrine loop and whether ARAF controls the expression and/or secretion of NRG1 in these cell types. However, one cannot rule out that ARAF regulates factors downstream of ERBB3 to control AKT signaling and cell survival, as this phenotype depends on its kinase activity. For instance, we identified PI3KR5, one of the regulatory subunits of class I PI3K gamma complex, being up-regulated in ARAF-depleted cells. This subunit has been shown to be required for G protein–mediated activation of this kinase (*26*) by recruiting its catalytic subunit p110γ to the plasma membrane, thereby facilitating downstream signaling via AKT. It is noteworthy that the ARAF-mediated suppression of AKT activation was not entirely explained by suppression of *ERBB3* expression. While the ERBB3 effect was independent of the kinase activity of ARAF, the suppression of AKT was not, suggesting a mechanistically different double protection by ARAF. The latter kinase-dependent mechanism points to a phosphorylation-dependent upstream regulator of Akt activation, possibly a phosphatase.

Further factors that are involved in the regulation of AKT/protein kinase B signaling comprise different members of the FGF receptor (FGFR) family. They are of special interest as they are up-regulated in both ARAF knockdown and kinase-deficient cells (Fig. 6). We have detected some changes in total AKT levels after depletion of BRAF and CRAF in A549 cells (Fig. 5, C and E), and further studies are warranted to check whether RAF isoforms control the stability and activity of AKT in these cell types. The FGFR signaling pathway is a key player in signal transduction in lung cancer not only because it controls various cellular functions such as cell cycle progression, migration, and survival but also because it activates signaling pathways that are involved in malignant tumor cell proliferation (*27*). Recent studies revealed a functional interplay between ERBB3 and FGFR-AKT signaling in up-regulating the metabolism of glioblastoma stem-like cells (*28*). Given the fact that FGFR inhibitors are currently investigated in clinical trials to treat lung cancers (*29*), it is an interesting avenue to explore whether ARAF directly regulates the expression of FGFR1 to FGFR3 in NSCLC.

We further identified regulations of Lyn, a Src family kinase, and MAP3K8 (Cot/Tpl2), a proto-oncogene in lung cancer, both of which are involved in cell-cell adhesion and were up-regulated in *ARAF* knockdown cells and in cells expressing kinase-impaired ARAF (*30*). While Lyn has been shown to regulate activation of EGFRs in LUAD cells by contributing to the formation of ERBB1/ERBB3/c-Myc complexes in the plasma membrane, aberrant transcriptional regulation and overexpression of MAP3K8 may be the common alteration that contributes to tumorigenic progression, possibly via AKT phosphorylation (*31*, *32*). In addition, DLC1, which suppresses NSCLC growth and invasion by RhoGAP-dependent and RhoGAP-independent mechanisms, was strongly down-regulated in ARAF-depleted cells (*27*). Experiments that identify DNA methylation patterns in the presence or absence of ARAF may provide further valuable insights into the mechanisms underlying these interesting observations in NSCLCs, contributing to tumor onset and extravasation up to metastatic spreading. Moreover, it would be interesting to investigate the mechanisms that lead to ARAF down-regulation in cell type– and tissue-specific manners beyond lung cancers. These data again highlight the importance of understanding the

tissue-specific role of "oncogenic" kinases in a kinase-dependent and kinase-independent manner to design rational therapies. Together, our observations disclose a clinically relevant ARAF-dependent suppression of ERBB3-AKT–driven lung cancer spreading that puts a brake on metastasis. ARAF depletion or dysfunction is therefore associated with poor prognosis.

MATERIALS AND METHODS

Cell culture

A549 cells (a gift from S. Horwitz and authenticated) were cultured in RPMI 1640 medium (Gibco BRL) supplemented with 10% fetal bovine serum (FBS) (Gibco BRL) and 0.2% penicillin (100 U/ml)/streptomycin (100 mg/ml) (Gibco BRL) at 37°C in 5% CO_2. NCI-H1650 (adenocarcinoma, mutant EGFR and WT KRAS), NCI-H1437 [adenocarcinoma, mutant MEK1(Q56P) and WT KRAS], NCI-H292 (KRAS WT), NCI-H226 (KRAS WT), Calu6 (KRAS mutated), NCI-H2122 (KRAS mutated), NCI-H441 (KRAS mutated), and NCI-H23 (KRAS mutated) were cultured as described for A549 (adenocarcinoma, EGFR-amplified and mutant KRAS G12S). Another A549 cell line was obtained from DSMZ. Where indicated, cells were treated with various concentrations (ranging from 25 to 100 ng/ml) of hNRG1 (catalog no. 5218, Cell Signaling Technology) or hEGF (40-217, NatuTec, Frankfurt am Main, Germany) at a final concentration of 100 ng/ml for 10 to 20 min. Dilutions of growth factors were done in phosphate-buffered saline (PBS) [10 mM sodium phosphate and 150 mM NaCl (pH 7.2)]. Selective MEK1/2 inhibitor trametinib (GSK1120212, catalog no. S2673, Selleckchem) was used at 1 μM working concentration for 1 hour, as was AKT inhibitor MK-2206 2HCl (catalog no. S1078, Selleckchem) and PI3K inhibitor (GDC-941). ERBB2/3 inhibitor sapitinib (AZD8931, catalog no. S2192) was applied in the presence of serum for the times and at the concentrations (ranging from 1 to 5 μM) indicated in the figures. Dimethyl sulfoxide (catalog no. A3672.0250, Applichem) was used as a solvent control for all inhibitors used.

Plasmids and constructs

Human full-length WT ARAF (ARAF-WT) cDNA was purified from Human Kinase Library (Addgene, catalog no. 23725). ARAF pDONR-223 was used as a template to generate ARAF-R362H, ARAF-K336M, and ARAF-S432A and kinase-deficient mutants and ARAF Y301D/Y302D (DD) kinase-active mutant. Site-directed mutagenesis was implemented by PCR using Q5 High-Fidelity DNA Polymerase (catalog no. MO491, New England BioLabs), and the following primers were used: ARAF R362H_fw, 5′-GTGCTCAGGAAGACGCACCATGTCAACATCTTG-3′; ARAF R362H_rev, 5′-CAAGATGTTGACATGGTGCGTCTTCCTGAGCAC-3′; ARAF K336M_fw, 5′-CATGGCGATGTGGCCGTGATGGTGCTCAAG-3′; ARAF K336M_rev, 5′-CTTGAGCACCATCACGGCCACATCGCCATG-3′; ARAF S432A_fw, 5′-CCACCGAGATCTCAAGGCTAACAACATCTTCCTAC-3′; ARAF S432A_rev, 5′-GTAGGAAGATGTTGTTAGCCTTGAGATCTCGGTGG-3′; ARAF Y301D/Y302D_fw, 5′-CGGGACTCAGGCGATGACTGGGAGGTACC-3′; ARAF Y301D/Y302D_rev, 5′-GGTACCTCCCAGTCATCGCCTGAGTCCCG-3′. For lentiviral expression, ARAF and the kinase mutant in pDONR-223 were transferred into the destination vector pLenti4TO/V5-Dest by clonase reaction (Gateway LR Clonase II Enzyme Mix, catalog no. 11791-020, Thermo Fisher Scientific).

Generation of knockdowns

shRNAs directed against human ARAF (NM_001654.1), human BRAF (NM_004333.2), or human CRAF (NM_002880.2) were obtained from Sigma-Aldrich. Cells were infected by lentiviral particles and subsequently selected for resistance to puromycin (2.5 μg/ml) until a stable knockdown culture was achieved. For complementation assays, the ARAF gene was reintroduced into shARAF [3′ untranslated region (3′UTR)] background by lentiviral infection [and selection with zeocin (200 μg/ml)]. Lentivirus particles were produced in human embryonic kidney 293T cells by transfecting cells with 1 μg of pLenti4TO/V5-DEST-ARAF and mutants (ARAF-R362H and ARAF-DD) together with 0.3 μg of viral packaging plasmids pHDM-G (encoding vesicular stomatitis virus glycoprotein), pHDM Hgpm2 (encoding codon-optimized HIV gag-pol proteins), pHDM tat 1b (encoding HIV Tat1b protein), and pRC cytomegalovirus (CMV)–Rev1b (encoding HIV rev protein) using GeneJuice transfection reagent (Merck Millipore, catalog no. 70967). After 2 days, the virus-containing medium was sterile-filtered, and cells were infected with lentiviral particles in the presence of polybrene (10 mg/ml; Merck Millipore). Cells were then double-selected for resistance to zeocin (100 μg/ml; Invivogen) and puromycin (5 μg/ml; Roth). The lentiviral particles with various shRNAs used for stable knockdown in A549 cells were as follows: hARAF shRNA (TRC no. 0000000567, 3′UTR region, CCGGCCAGCCAATCAATGTTCGTCTCTCGAGAGACGAACATTGATTGGCTGGTTTTT), hARAF shRNA (TRCN0000000571, CDS region, GACTCATCAAGGGACGAAAGA), hBRAF shRNA (TRC no. 0000006292, CDS region, CCGGCAGCAGTTACAAGCCTTCAAACTCGAGTTTGAAGGCTTGTAACTGCTGTTTTT), hCRAF shRNA (TRC no. 0000001067, CDS region CCGGCAAGCAAAGAACAGTGGTCAACTCGAGTTGACCACTGTTCTTTGCTTGTTTTT), and hKLF5 shRNA (TRC no. 0000013636) (CCGGCCCTGCCAGTTAACTCACAAACTCGAGTTTGTGAGTTAACTGGCAGGGTTTTT).

For the infection of other NSCLC cell lines, shRNAs plasmids were purified from the MISSION shRNA Human Library (Sigma-Aldrich) following the manufacturer's instructions. The nontargeting control shRNA (shCo) MISSION pLKO.1 puro (catalog no. SHC001) was included as a negative control.

Premade lentiviral particles expressing luciferase (Amsbio, #LVP326 blasticidin resistance; 10 μg/ml) were used to transduce A549 control (shCo) and ARAF-depleted (shARAF) cells for subsequent bioluminescence in vivo studies. In general, 1.8×10^5 infection units (IFU)/ml was used for lentiviral transduction following the protocol mentioned before.

To silence the expression of ARAF and BRAF together with CRAF by siRNA interference, approximately 75,000 cells per well were seeded in a 12-well plate at least 20 hours before transfection. The reverse transfection protocol was used for silencing ERBB3 transiently in accordance with the manufacturer's instructions. siRNAs directed against various genes and scrambled control siRNA as a negative control were transfected using Lipofectamine RNAiMAX (Invitrogen, catalog no. 13778) at a final concentration of 60 nM. Unless otherwise mentioned, cells were lysed at 48 hours after transfection to test efficiency. The following Hs_siRNAs were used in this study (sense strand sequence): siControl: 5′-UUCUCCGAACGUGUCACGU-3′ (QIAGEN, catalog no. 1027310); siARAF_5 (3′UTR): 5′-GACUCAAGGGACGAAA-3′ (QIAGEN, catalog no. SI00287686); siARAF_6 (CDS): 5′-GGGAUGGCAUGAGUGUCUA-3′ (QIAGEN, catalog no. S100287693); siBRAF: 5′-CAUAUAGAGGCCCUAUUGG-3′

(QIAGEN, catalog no. SI00299488); siCRAF (3′UTR): 5′-GGAUGUUGA-UGGUAGUACA-3′ (QIAGEN, custom-made); siERBB3: 5′-ACCACG-GTATCTGGTCATAAA-3′ (QIAGEN, catalog no. SI02660238); siKLF5: 5′-GAUUACCCUGGUUGCACA-3′ (Sigma-Aldrich/Merck, custom made). The knockdown was verified by SDS–polyacrylamide gel electrophoresis (PAGE) and, for ARAF, by quantitative real-time PCR.

Phospho-kinase array

To estimate relative levels of protein phosphorylation, the human Phospho-Kinase Array Kit (R&D Systems, no. ARY003B) was used, allowing for parallel detection of 43 kinase phosphorylation sites. Therefore, control and ARAF-depleted A549 cells (2.5×10^6) were seeded into adhesive cell culture plates and left for growing before processed further according to assay instructions. Briefly, after washing with PBS, the diluted cleared cell lysates (approximately 400 µg) were incubated overnight with the Human Phospho-Kinase array, which uses phospho-specific antibodies spotted in duplicates on nitrocellulose membranes. Following multiple washing steps to remove unbound protein, the array was incubated with a cocktail of biotinylated detection antibodies. To capture spots corresponding to the amount of phosphorylated protein, streptavidin–horseradish peroxidase (HRP) and chemiluminescent detection reagents were applied for signal detection. The analysis of spot pixel density was done with ImageJ software.

Colony formation assays

Agarose solution (1.5%) was mixed with 2× growth medium [with 20% fetal calf serum (FCS) and 2× inhibitor] to get a final mixture with 0.75% agarose in 1× growth medium (bottom agar medium). Bottom agar medium (1.5 ml) was added per well in a six-well plate and was left at room temperature to solidify. A549 cells stably expressing pLenti4TO/V5-DEST empty vector (EV) and pLenti4TO/V5-DEST-ARAF/R362H/DD were diluted in 2× growth medium (with 20% FCS and 2× inhibitors) and mixed with 0.9% agarose solution to a final concentration of 0.45% agarose. A total of 1.5 ml of this cell suspension was added to the bottom agarose layer (30 to 50,000 cells per condition). Cells seeded in soft agar were cultured for 2 to 3 weeks with addition of 100 µl of complete medium twice weekly. Colonies were stained with 0.02% crystal violet solution by gentle agitation at room temperature for about 1 to 2 hours followed by washes with water. The images were taken with a ChemiDoc Touch (Bio-Rad) imaging system, and the number of colonies was counted by ImageJ software.

Ninety-six–well soft agar colony formation assay

One-week 96-well soft agar colony formation assays were performed as described previously (*33*). The 1.5% agarose solution was mixed 1:1 with 2× RPMI medium supplemented with 20% FBS and left to solidify (50 µl of total volume per well-bottom layer). Top layer cell suspensions were prepared as follows (75 µl of total volume): 25 µl of 1.5% agarose, 25 µl of complete culture medium, and 25 µl of cell suspension containing 3000 cells. Top layer was added onto the bottom layer, and plates were incubated for 5 to 10 min at room temperature to allow polymerization before adding 125 µl of complete culture medium (1× RPMI with 10% FBS) containing twice the concentration of inhibitors (sapitinib, 1 or 5 µM, respectively) on top. Cells were seeded in triplicates.

After 7 days, cell growth and colony size in soft agar were determined by Hoechst 33342 staining (catalog no. H3570, Thermo Fisher Scientific) and subsequently quantified. Colonies were incubated with Hoechst (0.5 mg/ml) in PBS for 20 min at 37°C in a CO_2 incubator. Images were taken with a Leica DMi8 microscope (5× dry objective, Z-stack, 25 steps). Size of colonies was quantified by Fiji/ImageJ software using particle analyses ranging from 100 µm to infinity (300 µm to ∞).

In vivo luciferase imaging of tumor growth and metastases

A549 cells were stably transfected with the firefly luciferase gene, under the control of a strong CMV promotor, which leads to constitutive luciferase expression. One million cells per mouse and condition (±ARAF knockdown or reconstituted shARAF + kinase mutants) were suspended in cell culture medium and injected into the tail vein of 6- to 8-week-old nude female mice (Janvier, NMRI-nu). The in vivo studies included an exploratory test with each having two mice per groups (shARAF versus sh-Control) and two sets of experiments with each having six mice per group and condition. The first compared ARAF-depleted (shARAF) A549 cells with sh-Control-LUC cells (two groups), and the second also included shARAF-LUC to ensure reproducibility, plus a reconstituted "WT" (sh-ARAF-ARAF) and a kinase-deficient mutant (three groups). Luciferase activity was assessed repeatedly during the course of tumor development and metastases. In total, 13 mice of the control group and 11 mice in the ARAF-depleted group could be used for the end analysis. The mice had free access to food and water and were maintained in a climate-controlled room at a 12-hour light-dark cycle. Experiments were approved by the local ethics committee for animal research (Darmstadt, Germany) and were in line with the European and German regulations for animal research.

In vivo imaging was done with an IVIS Lumina Spectrum, which allows for analysis of bioluminescence and near-infrared signals, which were analyzed with LivingImage software (PerkinElmer). Bioluminescence was captured at 10 and 20 min after intraperitoneal injection of 100 µl of a solution (40 mg/ml) of XenoLight D-Luciferin-K+ salt (4 mg per mouse = 150 to 160 mg/kg). During imaging, mice were kept under 1 to 1.5% isoflurane anesthesia. The IVIS settings were as follows: Epi-bioluminescence, emission filter open, excitation filter block, fstop 1, binning 8, focus B 6.5 cm (close-up view of one to two mice with shielding of the tail), or focus C 13.2 cm (three mice), exposure of 60 s. Images were taken from the back and in ventral position to capture all metastases. Regions of interest (ROIs), i.e., the site of local tail tumor growth and metastatic regions, were identified by using the automatic detection tool implemented in LivingImage 4.3. For each mouse, the maximum time point of the total counts of bioluminescence in ROIs was used for statistical analysis of group differences, and groups were compared with parametric or nonparametric statistics depending on the data structure and distribution and using chi-squared statistics to assess the numbers of metastases.

Chromatin immunoprecipitation

Samples were sent to Active Motif (Carlsbad, CA) for ChIP-seq. Active Motif prepared chromatin, performed ChIP reactions, generated libraries, sequenced the libraries, and performed basic data analysis. Briefly, cells were fixed with 1% formaldehyde for 15 min and quenched with 0.125 M glycine. Chromatin was isolated by adding lysis buffer, followed by disruption with a Dounce homogenizer. Lysates were sonicated, and the DNA was sheared to an average length of 300 to 500 base pairs (bp) with Active Motif's EpiShear

probe sonicator (catalog no. 53051). Genomic DNA (input) was prepared by treating aliquots of chromatin with ribonuclease (RNase), proteinase K, and heat for decross-linking, followed by SPRI beads clean up (Beckman Coulter) and quantitation by Clariostar (BMG Labtech). Extrapolation to the original chromatin volume allowed determination of the total chromatin yield.

For each ChIP reaction, an aliquot of chromatin (30 μg) was precleared with protein A agarose beads (Invitrogen). Genomic DNA ROIs were isolated using 4 μg of antibody against KLF5 (Abcam, catalog no. ab137676, lot no. GR3312533-13). Complexes were washed, eluted from the beads with SDS buffer, and subjected to RNase and proteinase K treatment. Cross-links were reversed by incubation overnight at 65°C, and ChIP DNA was purified by phenol-chloroform extraction and ethanol precipitation.

qPCR reactions were carried out in triplicate on specific genomic regions using SYBR Green Supermix (Bio-Rad). The resulting signals were normalized for primer efficiency by carrying out qPCR for each primer pair using input DNA. The following primers were used: h ERBB3_-234A, AACCGGCTAGGGGAGTTGAG; h ERBB3_-234B, AAGGGTAATGAATGAGGGAGTG; h ERBB3_+97A, AGGCTCCGCAATCCCTACTC; h ERBB3_+97B, GGGGTGTGTGTGTGTGAGAG; h ERBB3_+10A, AAATTAGGGTGAGCCCCATC; h ERBB3_+10B, GAGGCTGGAGTAGGGATTGC; h ERBB3_-258A, CTGAGAGAAAATCCACCAAGTG; h ERBB3_-258B, TCGCCCATTAACCAAATCAC; h ERBB3_+280A, ACCCTCTGCGGAGTCATGAG; h ERBB3_+280B, GCCACTTACCTGCCTGAGAG; h PLXNA2_+59KA, GGCCAGCCCTAGATAATGTG; h PLXNA2_+59KB, CCTTCCATCCCTGCCTACAC.

Antibodies

Anti–V5-tag antibody (#13202), anti–phospho-p44/42 MAPK (Thr^{202}/Tyr^{204}) antibody (#9101L), anti- p44/42 MAPK antibody (#9102), anti–phospho-MEK1/2 ($Ser^{217/221}$) antibody (41G9) (#9154), anti-MEK1 (61B12) antibody (#2352), anti–phospho-Akt (Thr^{308}) antibody (#9275), anti–phospho-Akt (Ser^{473}) antibody (#4060), anti-Akt antibody (pan) (C67E7, #4691), anti–phospho-EGFR (Y1068) antibody (#3777), anti-EGFR receptor (D38B1) antibody (#4267), anti–phospho-HER3/ErbB3 (Tyr^{1289}) (21D3) antibody (#4791), anti-HER3/ERBB3 (D22C5) XP antibody (#12708), anti-FoxC1 (D8A6) antibody (#8758), and anti-KLF5 (D7S3F) antibody (#51586) were purchased from Cell Signaling Technology (Danvers, MA, USA). Anti-ARAF antibody (catalog no. sc-408), anti-BRAF antibody (catalog no. sc-5284), and anti-CRAF antibody (catalog no. sc-133) were obtained from Santa Cruz. Anti-vinculin antibody (catalog no. SAB4200080) was purchased from Sigma-Aldrich. Anti–M2-PK antibody (S-1) was purchased from Schebo Biotech AG. HRP-conjugated secondary antibodies for rabbit immunoglobulin G were obtained from Novex (Boston, MA, USA; A16096) and Thermo Fisher Scientific (#32460).

Western blotting

Cells were washed with ice-cold PBS [10 mM sodium phosphate and 150 mM NaCl (pH 7.2)], lysed in 2× Laemmli buffer [0.125 M tris-HCl (pH 6.8), 4% SDS, and 10% glycerol] supplemented with 50 mM dithiothreitol (DTT) per each 1 ml of buffer, and boiled at 100°C for 5 min before subjected to 7.5% SDS-PAGE followed by transfer of the proteins onto nitrocellulose membranes (GE Healthcare, Chalfont St. Giles, UK). Membranes were blocked in 3% bovine serum albumin/PBST [1× PBS (pH 7.2) containing 0.05% Tween 20] for 1 hour at room temperature and, after 3 × 5 min, PBST-wash incubated overnight with primary antibody diluted in PBST at 4°C. Following 3 × 5 min of washing with PBST, membranes were incubated with HRP-conjugated secondary antibody for 1 hour at room temperature, and after subsequent washing, antigen/antibody complexes were visualized by enhanced chemiluminescence (Immobilon Western, catalog no. WBKLS0500, Merck Millipore). Quantification of Western blots was performed by densitometry with ImageJ software (National Institutes of Health). For indicated experiments, cells were washed with ice-cold 1× PBS [10 mM sodium phosphate and 150 mM NaCl (pH 7.2)] and lysed for 20 min in cold radioimmunoprecipitation assay (RIPA) lysis buffer [250 mM NaCl, 50 mM tris (pH 7.5), 10% glycerine, and 1% Triton X-100], supplemented with protease inhibitor cocktail Set I-Calbiochem 1:100 (catalog no. 539131, Merck Millipore) and phosphatase inhibitors [1 mM sodium orthovanadate (Na_3VO_4) and 1 mM sodium fluoride (NaF)] followed by 10 min of centrifugation at 14,000 rpm. Protein concentrations were estimated using 660-nm Protein Assay (catalog no. 22660, Thermo Fisher Scientific), and 45 μg of protein extract was subjected to SDS-PAGE as mentioned before.

Immunoprecipitation

To immunoprecipitate reconstituted ARAF protein (V5 tagged) in A549 cells that were depleted for ARAF, 3×10^6 cells were lysed in 500 to 800 μl of IP buffer (100 mM NaCl, 50 mM tris-Cl, 1% NP-40, 1 mM $NaVO_3$, 1 mM NaF, and 1× protease inhibitor) for 30 min on ice. After clearing the lysates by centrifugation for 15 min at 14,000 rpm (at 4°C), the protein concentration was determined using Pierce 660-nm Protein Assay Reagent (catalog no. 22660, Thermo Fisher Scientific). Reconstituted ARAF (WT and kinase-deficient mutants) was immunoprecipitated from 500 μg of total protein by overnight incubation (4°C) with V5 antibody and the subsequent precipitation of the antigen-antibody complexes by agarose-coupled protein A/G beads (catalog no. 11-134-515-001 and 11-243-233-001, Roche). Beads were washed with IP buffer, and bound proteins were subjected for further analyses.

RAF kinase assay

Kinase activity of V5-tagged ARAF-WT and ARAF kinase-deficient mutants (ARAF-R362H, ARAF-S432A, ARAF-K336M, and ARAF-D447N) was investigated. Constructs were stably overexpressed in ARAF-depleted A549 cells and immunoprecipitated via the V5 tag as described before. The EV (shARAF + EV) served as a control. Agarose-coupled protein A/G beads were used to precipitate the antibody/antigen complexes to which a reaction mix of 1× kinase buffer [10× buffer: 100 mM $MgCl_2$, 250 mM β-glycerolphosphate, 250 mM Hepes (pH 7.5), 50 mM benzamidine, 5 mM DTT, and 10 mM $NaVO_3$; diluted to 1× with H_2O] and 1 μg of kinase-dead His-MEK1 K97A (catalog no. M02-16H, SignalChem) was added in a total volume of 38 μl. After adding MgATP (Enzo Life Sciences; stock, 20×; diluted to 1×), the reaction was incubated at 30°C for 30 min before it was stopped by the addition of 10 μl of Laemmli buffer. The entire reaction mix was loaded on SDS-PAGE gel for immunoblot analysis.

RNA isolation, cDNA synthesis, and RT-PCR analysis

For gene expression analysis, cells were washed with cold PBS, and total RNA was extracted using TRIzol (catalog no. 15596018, Ambion) according to the manufacturer's instructions. RNA quality was

evaluated by NanoDrop (Thermo Fisher Scientific) measurements (absorbance, 260/280), and samples within the range of 2.0 ± 0.3 were taken for cDNA synthesis. Isolated RNA (500 ng) was used as a template for cDNA synthesis using the RevertAid First Strand cDNA synthesis kit (catalog no. K1621, Thermo Fisher Scientific) and random hexamer primers.

Real-time PCR was performed using EvaGreen qPCR master mix [5× Hot Start Taq EvaGreen qPCR Mix (no ROX), catalog no. 27490, Axon] and the following primers: ERBB3 fw_5′ CTGCTGCCTC CTGATGATAA; ERBB3 rev_5′ ACTCCCAAACTGTCACACCA; ARAF fw_5′ CTACGACTCTCTAGACAAGG; ARAF rev_5′ GTACAAAATTGTGCATGGTC; KLF5 fw_5′ TTTGGAGAAACGACGCATCC; KLF5 rev_5′ GTGAGTCCTCAGGTGAGCTT.

The housekeeping gene GAPDH was used for normalization: GAPDH fw_5′ CGACAGTCAGCCGCATCTT and GAPDH rev_5′ CCCCATGGTGTCTGAGCG. Relative expression levels were calculated as $\Delta\Delta C_t$, and results are presented as $\log_2$ fold difference in gene expression (fold change).

RNA-seq and bioinformatic analyses

Two biological replicates of A549 cells (ARAF depleted ± ARAF-WT ARAFR362H) were seeded in adhesive cell culture dishes at an initial density of 2×10^5 cells per well and, 48 hours later, washed with cold 1× PBS and subjected to RNA isolation (High Pure RNA Isolation kit, catalog no.11828665001, Roche) according to the manufacturer's instructions. Total RNA was quantified by a Qubit 2.0 fluorometer (Invitrogen), and quality was assessed using Agilent's bioanalyzer 2100 and an RNA 6000 Nano chip (Agilent). Samples with RNA integrity number > 8 were further subjected for RNA library preparation. Barcoded cDNA libraries were prepared from 500 ng of total RNA using the NEBnext Poly(A) mRNA Magnetic Isolation Module and NEBNext Ultra RNA Library Prep Kit for Illumina (NEB) according to the manufacturer's instruction. Library quantity was assessed on a Qubit 2.0 using Invitrogen's Qubit HS assay kit, and the library size was determined using Agilent's bioanalyzer 2100 and an HS DNA assay chip. Barcoded RNA-seq libraries were on-board clustered using the HiSeq Rapid SR Cluster Kit v2 ith 8 pM, and 1 × 51 bp were sequenced on an Illumina HiSeq2500 using a HiSeq Rapid SBS kit v2.

Quality control on the sequencing data (51 bp, single end) was performed with the FastQC tool (available at www.bioinformatics.babraham.ac.uk/projects/fastqc/), as well as the comprehensive Qorts suite. By inspecting the produced reports, all samples were deemed of good quality and were included in the analysis. Short reads alignment was performed with the ENSEMBL Homo_sapiens.GRCh38 that was chosen as the reference genome. The corresponding annotation (ENSEMBL v82, Homo_sapiens.GRCh38.82.gtf) was retrieved from the ENSEMBL FTP website (www.ensembl.org/info/data/ftp/index.html). The STAR aligner (version 2.4.0j) was used to perform mapping to the reference genome (*29*). Subsequent analyses were performed with R statistical software (version 3.6.0), leveraging core packages of the Bioconductor project.

Alignments were processed with the "featureCounts" function of the Rsubread package, using the annotation file, which was also used for the alignment. Exploratory data and PCA and functional annotation to GO terms were performed with the pcaExplorer package [version 2.12.0 (*34*)] and with the clusterProfiler package (version 3.14.0) (*35*).

Differential expression analysis was performed with the DESeq2 package (version 1.26.0), limiting the false discovery rate to 0.05 (*36*). The apeglm (package version 1.8.0) shrinkage estimator was used to calculate the effect size for the contrasts of interest (*37*). MA plots were generated with the ideal package (version 1.10.0) (*33*).

Gene expression profiles were plotted as heatmaps [color-coded *z* scores for the regularized logarithm (rlog)–transformed expression values] with the pheatmap package (version 1.0.12). Expression plots for selected genes display the individual values for the normalized counts.

Analysis of publicly available data

TCGA processed gene expression data and clinical information for LUAD were downloaded from the UCSC cancer genome browser. GSE37745 processed gene expression and clinical information for LUAD were also downloaded from Gene Expression Omnibus (*38*). Nonredundant set of samples was kept for further survival analysis. Survival analysis was performed using R packages survminer and Survival. Optimal cutoff for ARAF high and low expression was obtained using surv_cutpoint function. TCGA gene expression data were also retrieved via the curated TCGA Data package (version 1.8.0) and processed with TCGAUtils (version 1.6.1) for further analysis. For analyzing ARAF expression, the normalized counts were used after $\log_2$ transformation (after adding a pseudocount of 1). Clinical information on the KRAS and EGFR mutation status was retrieved from the UCSC Cancer Genomics Browser (https://genome-cancer.ucsc.edu/).

ERBB3 promoter luciferase reporter assay

The ERBB3-Gaussia Luciferase GLuc-ON promoter reporter clone was purchased from Addgene (#60899) as a lentiviral expression construct along with the negative control plasmids (PEZX-LvPG02, GeneCopeia) with nonpromoter sequence. Unless otherwise stated, 250,000 A549 cells stably transfected with shRNA targeting ARAF at 3′UTR (shARAF) or with control EV shRNA were transiently transfected with 1 μg of ERBB3 Gaussia Luciferase construct (GLuc-ON promotor reporter clone) and negative control plasmids, respectively (duplicates), in the presence of 5.4 μl of polyethylenimine (Polysciences Inc., catalog no. 23966) at a concentration of 10 mM. Twenty-four hours after transfection, medium was exchanged for RPMI-FBS, and cells were cultured for an additional 24 hours. Cells were washed with ice-cold PBS [10 mM sodium phosphate and 150 mM NaCl (pH 7.2)] and lysed with 250 μl of 1× passive lysis buffer (Promega, catalog no. E1910) for 15 min at room temperature. The lysates were cleared by top spin centrifugation (at 4°C), and the protein concentration was determined using Pierce 660-nm Protein Assay Reagent (catalog no. 22660, Thermo Fisher Scientific). Fifteen to 25 μg of protein in a total volume of 30 μl was mixed with 10 μl of luciferase assay substrate (LAR II) in a 96-well plate, and ERBB3 promoter activity was assessed by measurement of luciferase activity according to the supplied user manual (Promega, catalog no. E1910). Relative luminescence units (RLU) were measured (integration, 1 s) using a Tecan reader, and RLU values of negative control were subtracted from ERBB3 promoter–expressing samples for quantification. ERBB3 promoter activity in ARAF-depleted cells was presented as fold change normalized to shCo samples or shARAF + ARAF, respectively.

Immunohistochemistry

IHC staining of ARAF, p-Akt, and ERBB3 in NSCLC patient samples was performed, and all ethical permissions for the collection of these patient samples were obtained by Indivumed GmbH (Hamburg, Germany). Tissue microarrays (TMAs) were used for staining of

LUSC (ARAF: n = 41; p-Akt: n = 26; ERBB3: n = 28 spots) and LUAD (ARAF: n = 43 spots; p-Akt: n = 19 spots; ERBB3: n = 19 spots) including matching tumor-adjacent normal tissue (ARAF: n = 13 spots; p-Akt: n = 10 spots; ERBB3: n = 10 spots). IHC was implemented on the Discovery XT and BenchMark Ultra staining platform (Roche Diagnostics, Mannheim, Germany/Ventana Medical Systems). The following primary antibodies were used: anti-ARAF (0.5 µg/ml; catalog no. Ab200653, Abcam), anti–p-Akt (4.3 µg/ml; catalog no. 4060, Cell Signaling Technology), and anti-ERBB3 (0.5 µg/ml; catalog no. 12708, Cell Signaling Technology). Isotype controls were prepared for each sample. After slicing formalin-fixed paraffin-embedded TMAs into 3-µm sections, they were mounted on TOMO glass slides (Matsunami). Hematoxylin and eosin–stained sections were prepared according to Indivumed's standard operating procedure. The slides were deparaffinized within the staining instrument, and the heat-induced epitope retrieval was conducted in citrate buffer (pH 6) for anti–A-Raf staining and in EDTA buffer (pH 8.5) for anti–p-Akt and anti-ERBB3 staining. After a blocking step with 2% normal goat serum (ARAF: 20 min; p-Akt: 32 min; ERBB3: 8 min), all samples were incubated with the primary antibodies (ARAF: 32 min, room temperature; p-Akt: 32 min, 37°C; ERBB3: 1 hour, 37°C). The ultraView Universal DAB Detection Kit (Roche Diagnostics) was used to immunostain against ARAF, whereas the Discovery ChromoMap DAB Kit (Roche Diagnostics) and the Discovery OmniMap anti-rabbit HRP secondary antibody were used to immunostain the slides against p-Akt and ERBB3. Afterward, the slides were counterstained using Hematoxylin II and Bluing Reagent (Roche Diagnostics, Mannheim, Germany/Ventana Medical Systems).

The IHC stainings were semiquantitatively evaluated by Indivumed's pathologist and were analyzed using the H-score classification as described in the literature for estrogen receptor (*39*). The percentages of weakly, moderately, and strongly stained tumor cells or normal epithelial cells (pneumocytes) for tumor-adjacent normal tissue were estimated, and the H-score was calculated according to the following formula: H-score = (weak)% + (moderate)% × 2 + (strong)% × 3. The table below shows the H-score classification based on the resulting score ranges from 0 to 300.

Table 1. H-score classification.

H-score	Classification
0–50	Negative
51–100	Weakly positive
101–200	Moderately positive
201–300	Strongly positive

IHC—Tissue mice

For IHC staining of paraffin-embedded tumor tissue, antibodies directed against P-Akt (Ser^{473}, Cell Signaling Technology) and Ki67 (MIB-1, Dako) were used. All slides were stained with automatized immunostainers (Autostainer plus, Dako) according to standard procedures. For the IHC semiquantitative assessment of P-Akt expression, the product of the scores of staining intensity and quantity of immunoreactive tumor cells was calculated on the basis of the following scoring system: The intensity ranged from 0, negative; 1, low; 2, medium; to 3, high; the quantity composed of 0, no expression; 1, positivity in 1 to 25%; 2, positivity in 26 to 50%; 3, positivity in 51 to 75%; and 4, positivity in >75%. The final IHC score (ranging from 0 to 12) is obtained by multiplication of the intensity score and the quantity score.

Statistical analyses

Data are presented as means ± SD or means ± SEM as specified in the figure legends. Statistical analyses were done with GraphPad Prism 5.0. Groups were compared with nonparametric tests for not normally distributed data (Mann-Whitney) or parametric tests including two-sided, unpaired or paired (for fold changes) Student's t tests or analyses of variance (ANOVAs; one-way). In case of significant ANOVA results, groups were subsequently compared by t tests using an adjustment of alpha according to Bonferroni to account for multiple comparisons. P values lower than 0.05 were considered as a significant difference. Further analyses included chi-square statistics to compare the frequency of metastases and Kaplan-Meier survival analyses.

SUPPLEMENTARY MATERIALS

Supplementary material for this article is available at https://science.org/doi/10.1126/sciadv.abk1538

View/request a protocol for this paper from *Bio-protocol*.

REFERENCES AND NOTES

1. S. Dearden, J. Stevens, Y. L. Wu, D. Blowers, Mutation incidence and coincidence in non small-cell lung cancer: Meta-analyses by ethnicity and histology (mutMap). *Ann. Oncol.* **24**, 2371–2376 (2013).
2. H. Lavoie, M. Therrien, Regulation of RAF protein kinases in ERK signalling. *Nat. Rev. Mol. Cell Biol.* **16**, 281–298 (2015).
3. D. Matallanas, M. Birtwistle, D. Romano, A. Zebisch, J. Rauch, A. von Kriegsheim, W. Kolch, Raf family kinases: Old dogs have learned new tricks. *Genes Cancer* **2**, 232–260 (2011).
4. M. Raman, W. Chen, M. H. Cobb, Differential regulation and properties of MAPKs. *Oncogene* **26**, 3100–3112 (2007).
5. C. Wellbrock, M. Karasarides, R. Marais, The RAF proteins take centre stage. *Nat. Rev. Mol. Cell Biol.* **5**, 875–885 (2004).
6. K. Rajalingam, R. Schreck, U. R. Rapp, Š. Albert, Ras oncogenes and their downstream targets. *Biochim. Biophys. Acta* **1773**, 1177–1195 (2007).
7. C. K. Weber, J. R. Slupsky, H. A. Kalmes, U. R. Rapp, Active Ras induces heterodimerization of cRaf and BRaf. *Cancer Res.* **61**, 3595–3598 (2001).
8. H. Davies, G. R. Bignell, C. Cox, P. Stephens, S. Edkins, S. Clegg, J. Teague, H. Woffendin, M. J. Garnett, W. Bottomley, N. Davis, E. Dicks, R. Ewing, Y. Floyd, K. Gray, S. Hall, R. Hawes, J. Hughes, V. Kosmidou, A. Menzies, C. Mould, A. Parker, C. Stevens, S. Watt, S. Hooper, R. Wilson, H. Jayatilake, B. A. Gusterson, C. Cooper, J. Shipley, D. Hargrave, K. Pritchard-Jones, N. Maitland, G. Chenevix-Trench, G. J. Riggins, D. D. Bigner, G. Palmieri, A. Cossu, A. Flanagan, A. Nicholson, J. W. C. Ho, S. Y. Leung, S. T. Yuen, B. L. Weber, H. F. Seigler, T. L. Darrow, H. Paterson, R. Marais, C. J. Marshall, R. Wooster, M. R. Stratton, P. A. Futreal, Mutations of the BRAF gene in human cancer. *Nature* **417**, 949–954 (2002).
9. I. Yen, F. Shanahan, J. Lee, Y. S. Hong, S. J. Shin, A. R. Moore, J. Sudhamsu, M. T. Chang, I. Bae, D. D. Cruz, T. Hunsaker, C. Klijn, N. P. D. Liau, E. Lin, S. E. Martin, Z. Modrusan, R. Piskol, E. Segal, A. Venkatanarayan, X. Ye, J. Yin, L. Zhang, J.-S. Kim, H.-S. Lim, K.-P. Kim, Y. J. Kim, H. S. Han, S. J. Lee, S. T. Kim, M. Jung, Y.-H. Hong, Y. S. Noh, M. Choi, O. Han, M. Nowicka, S. Srinivasan, Y. Yan, T. W. Kim, S. Malek, ARAF mutations confer resistance to the RAF inhibitor belvarafenib in melanoma. *Nature* **594**, 418–423 (2021).
10. J. Rauch, K. Moran-Jones, V. Albrecht, T. Schwarzl, K. Hunter, O. Gires, W. Kolch, c-Myc regulates RNA splicing of the A-Raf kinase and its activation of the ERK pathway. *Cancer Res.* **71**, 4664–4674 (2011).
11. J. Mooz, T. K. Oberoi-Khanuja, G. S. Harms, W. Wang, B. S. Jaiswal, S. Seshagiri, R. Tikkanen, K. Rajalingam, Dimerization of the kinase ARAF promotes MAPK pathway activation and cell migration. *Sci. Signal.* **7**, ra73 (2014).
12. K. A. Monaco, S. Delach, J. Yuan, Y. Mishina, P. Fordjour, E. Labrot, D. McKay, R. Guo, S. Higgins, H. Q. Wang, J. Liang, K. Bui, J. Green, P. Aspesi, J. Ambrose, F. Mapa, L. Griner, M. Jaskelioff, J. Fuller, K. Crawford, G. Pardee, S. Widger, P. S. Hammerman, J. A. Engelman, D. D. Stuart, V. G. Cooke, G. Caponigro, LXH254, a potent and selective ARAF-sparing

inhibitor of BRAF and CRAF for the treatment of MAPK-driven tumors. *Clin. Cancer Res.* **27**, 2061–2073 (2021).
13. J. Rauch, D. Vandamme, B. Mack, B. McCann, N. Volinsky, A. Blanco, O. Gires, W. Kolch, Differential localization of A-Raf regulates MST2-mediated apoptosis during epithelial differentiation. *Cell Death Differ.* **23**, 1283–1295 (2016).
14. M. Imielinski, H. Greulich, B. Kaplan, L. Araujo, J. Amann, L. Horn, J. Schiller, M. A. Villalona-Calero, M. Meyerson, D. P. Carbone, Oncogenic and sorafenib-sensitive ARAF mutations in lung adenocarcinoma. *J. Clin. Invest.* **124**, 1582–1586 (2014).
15. D. Li, M. E. March, A. Gutierrez-Uzquiza, C. Kao, C. Seiler, E. Pinto, L. S. Matsuoka, M. R. Battig, E. J. Bhoj, T. L. Wenger, L. Tian, N. Robinson, T. Wang, Y. Liu, B. M. Weinstein, M. Swift, H. M. Jung, C. N. Kaminski, R. Chiavacci, J. A. Perkins, M. A. Levine, P. M. A. Sleiman, P. J. Hicks, J. T. Strausbaugh, J. B. Belasco, Y. Dori, H. Hakonarson, ARAF recurrent mutation causes central conducting lymphatic anomaly treatable with a MEK inhibitor. *Nat. Med.* **25**, 1116–1122 (2019).
16. K. A. Olaussen, F. Commo, M. Tailler, L. Lacroix, I. Vitale, S. Q. Raza, C. Richon, P. Dessen, V. Lazar, J.-C. Soria, G. Kroemer, Synergistic proapoptotic effects of the two tyrosine kinase inhibitors pazopanib and lapatinib on multiple carcinoma cell lines. *Oncogene* **28**, 4249–4260 (2009).
17. K. Riegel, J. Schlöder, M. Sobczak, H. Jonuleit, B. Thiede, H. Schild, K. Rajalingam, RAF kinases are stabilized and required for dendritic cell differentiation and function. *Cell Death Differ.* **27**, 1300–1315 (2020).
18. P. Workman, P. A. Clarke, F. I. Raynaud, R. L. M. van Montfort, Drugging the PI3 kinome: From chemical tools to drugs in the clinic. *Cancer Res.* **70**, 2146–2157 (2010).
19. J. Ma, H. Lyu, J. Huang, B. Liu, Targeting of erbB3 receptor to overcome resistance in cancer treatment. *Mol. Cancer* **13**, 105 (2014).
20. S. Cao, Z. Wang, X. Gao, W. He, Y. Cai, H. Chen, R. Xu, FOXC1 induces cancer stem cell-like properties through upregulation of beta-catenin in NSCLC. *J. Exp. Clin. Cancer Res.* **37**, 220 (2018).
21. I. Jeric, G. Maurer, A. L. Cavallo, J. Raguz, E. Desideri, B. Tarkowski, M. Parrini, I. Fischer, K. Zatloukal, M. Baccarini, A cell-autonomous tumour suppressor role of RAF1 in hepatocarcinogenesis. *Nat. Commun.* **7**, 13781 (2016).
22. C. Montero-Conde, S. Ruiz-Llorente, J. M. Dominguez, J. A. Knauf, A. Viale, E. J. Sherman, M. Ryder, R. A. Ghossein, N. Rosen, J. A. Fagin, Relief of feedback inhibition of HER3 transcription by RAF and MEK inhibitors attenuates their antitumor effects in BRAF-mutant thyroid carcinomas. *Cancer Discov.* **3**, 520–533 (2013).
23. E. V. Abel, K. J. Basile, C. H. Kugel III, A. K. Witkiewicz, K. le, R. K. Amaravadi, G. C. Karakousis, X. Xu, W. Xu, L. M. Schuchter, J. B. Lee, A. Ertel, P. Fortina, A. E. Aplin, Melanoma adapts to RAF/MEK inhibitors through FOXD3-mediated upregulation of ERBB3. *J. Clin. Invest.* **123**, 2155–2168 (2013).
24. R. B. Blasco, S. Francoz, D. Santamaría, M. Cañamero, P. Dubus, J. Charron, M. Baccarini, M. Barbacid, c-Raf, but not B-Raf, is essential for development of K-Ras oncogene-driven non-small cell lung carcinoma. *Cancer Cell* **19**, 652–663 (2011).
25. G. Sithanandam, L. W. Fornwald, J. Fields, L. M. Anderson, Inactivation of ErbB3 by siRNA promotes apoptosis and attenuates growth and invasiveness of human lung adenocarcinoma cell line A549. *Oncogene* **24**, 1847–1859 (2005).
26. C. Brock, M. Schaefer, H. P. Reusch, C. Czupalla, M. Michalke, K. Spicher, G. Schultz, B. Nürnberg, Roles of Gβγ in membrane recruitment and activation of p110γ/p101 phosphoinositide 3-kinase γ. *J. Cell Biol.* **160**, 89–99 (2003).
27. K. D. Healy, L. Hodgson, T. Y. Kim, A. Shutes, S. Maddileti, R. L. Juliano, K. M. Hahn, T. K. Harden, Y. J. Bang, C. J. der, DLC-1 suppresses non-small cell lung cancer growth and invasion by RhoGAP-dependent and independent mechanisms. *Mol. Carcinog.* **47**, 326–337 (2008).
28. F. De Bacco, F. Orzan, J. Erriquez, E. Casanova, L. Barault, R. Albano, A. D'Ambrosio, V. Bigatto, G. Reato, M. Patanè, B. Pollo, G. Kuesters, C. Dell'Aglio, L. Casorzo, S. Pellegatta, G. Finocchiaro, P. M. Comoglio, C. Boccaccio, ERBB3 overexpression due to miR-205 inactivation confers sensitivity to FGF, metabolic activation, and liability to ERBB3 targeting in glioblastoma. *Cell Rep.* **36**, 109455 (2021).
29. A. Dobin, C. A. Davis, F. Schlesinger, J. Drenkow, C. Zaleski, S. Jha, P. Batut, M. Chaisson, T. R. Gingeras, STAR: Ultrafast universal RNA-seq aligner. *Bioinformatics* **29**, 15–21 (2013).
30. A. M. Clark, S. H. Reynolds, M. Anderson, J. S. Wiest, Mutational activation of the MAP3K8 protooncogene in lung cancer. *Genes Chromosomes Cancer* **41**, 99–108 (2004).
31. P. Sutton, J. A. Borgia, P. Bonomi, J. M. D. Plate, Lyn, a Src family kinase, regulates activation of epidermal growth factor receptors in lung adenocarcinoma cells. *Mol. Cancer* **12**, 76 (2013).
32. C. M. Johannessen, J. S. Boehm, S. Y. Kim, S. R. Thomas, L. Wardwell, L. A. Johnson, C. M. Emery, N. Stransky, A. P. Cogdill, J. Barretina, G. Caponigro, H. Hieronymus, R. R. Murray, K. Salehi-Ashtiani, D. E. Hill, M. Vidal, J. J. Zhao, X. Yang, O. Alkan, S. Kim, J. L. Harris, C. J. Wilson, V. E. Myer, P. M. Finan, D. E. Root, T. M. Roberts, T. Golub, K. T. Flaherty, R. Dummer, B. L. Weber, W. R. Sellers, R. Schlegel, J. A. Wargo, W. C. Hahn, L. A. Garraway, COT drives resistance to RAF inhibition through MAP kinase pathway reactivation. *Nature* **468**, 968–972 (2010).
33. F. Marini, J. Linke, H. Binder, ideal: An R/Bioconductor package for interactive differential expression analysis. *BMC Bioinformatics* **21**, 565 (2020).
34. F. Marini, H. Binder, pcaExplorer: An R/Bioconductor package for interacting with RNA-seq principal components. *BMC Bioinformatics* **20**, 331 (2019).
35. G. Yu, L.-G. Wang, Y. Han, Q.-Y. He, clusterProfiler: An R package for comparing biological themes among gene clusters. *OMICS* **16**, 284–287 (2012).
36. M. I. Love, W. Huber, S. Anders, Moderated estimation of fold change and dispersion for RNA-seq data with DESeq2. *Genome Biol.* **15**, 550 (2014).
37. A. Zhu, J. G. Ibrahim, M. I. Love, Heavy-tailed prior distributions for sequence count data: Removing the noise and preserving large differences. *Bioinformatics* **35**, 2084–2092 (2019).
38. T. Barrett, S. E. Wilhite, P. Ledoux, C. Evangelista, I. F. Kim, M. Tomashevsky, K. A. Marshall, K. H. Phillippy, P. M. Sherman, M. Holko, A. Yefanov, H. Lee, N. Zhang, C. L. Robertson, N. Serova, S. Davis, A. Soboleva, NCBI GEO: Archive for functional genomics data sets—Update. *Nucleic Acids Res.* **41**, D991–D995 (2013).
39. K. S. McCarty Jr., L. S. Miller, E. B Cox, J. Konrath, K. S. McCarty Sr., Estrogen receptor analyses. Correlation of biochemical and immunohistochemical methods using monoclonal antireceptor antibodies. *Arch. Pathol. Lab. Med.* **109**, 716–721 (1985).

Acknowledgments: We would like to thank the Active Motif team for the CHIP-qPCR experiments. We thank S. Wenzel for technical assistance. We thank D. Hoeller for critically reading the manuscript. **Funding:** The work is supported by grants from the DFG to K.Ra. (CRC1292, RA1939/8-1, and GFK fellowship). **Author contributions:** Conception and/or design of the work: J.M., K.Ri., A.S., I.T., W.R., and K.Ra. Acquisition, analysis, and/or interpretation of data: J.M., K.Ri., H.P.S., A.S., F.M., M.K., U.W., W.R., A.W.-S., I.T., K.Ra. Drafted the work or substantively revised it: J.M., K.Ri., and K.Ra. with input from all authors. **Competing interests:** The authors declare that they have no competing interests. **Data and materials availability:** All data needed to evaluate the conclusions in the paper are present in the paper and/or the Supplementary Materials.

Submitted 24 June 2021
Accepted 27 January 2022
Published 18 March 2022
10.1126/sciadv.abk1538